HHS Public Access

Author manuscript

Cell Rep. Author manuscript; available in PMC 2024 May 09.

Published in final edited form as:

Cell Rep. 2024 April 23; 43(4): 114072. doi:10.1016/j.celrep.2024.114072.

Functionally diverse thymic medullary epithelial cells interplay to direct central tolerance

Aya Ushio[1,2,6], **Mami Matsuda-Lennikov**[1,6], **Felix Kalle-Youngoue**[1,3], **Akihide Shimizu**[1], **Abdalla Abdelmaksoud**[4], **Michael C. Kelly**[5], **Naozumi Ishimaru**[2], **Yousuke Takahama**[1,7,*]

[1]Thymus Biology Section, Experimental Immunology Branch, National Cancer Institute, National Institutes of Health, Bethesda, MD 20892, USA

[2]Department of Oral Molecular Pathology, Graduate School of Biomedical Sciences, Tokushima University, Kuramoto, Tokushima 770-8504, Japan

[3]Frederick National Laboratory for Cancer Research, National Cancer Institute, National Institutes of Health, Frederick, MD 21701, USA

[4]Center for Cancer Research Collaborative Bioinformatics Resource, National Cancer Institute, National Institutes of Health, Bethesda, MD 20892, USA

[5]Single Cell Analysis Facility, Cancer Research Technology Program, National Cancer Institute, National Institutes of Health, Bethesda, MD 20892, USA

[6]These authors contributed equally

[7]Lead contact

SUMMARY

Medullary thymic epithelial cells (mTECs) are essential for the establishment of self-tolerance in T cells. Promiscuous gene expression by a subpopulation of mTECs regulated by the nuclear protein Aire contributes to the display of self-genomic products to newly generated T cells. Recent reports have highlighted additional self-antigen-displaying mTEC subpopulations, namely Fezf2-expressing mTECs and a mosaic of self-mimetic mTECs including thymic tuft cells. In addition, a functionally different subset of mTECs produces chemokine CCL21, which attracts developing thymocytes to the medullary region. Here, we report that $CCL21^+$ mTECs and $Aire^+$ mTECs non-redundantly cooperate to direct self-tolerance to prevent autoimmune pathology by optimizing the deletion of self-reactive T cells and the generation of regulatory T cells. We also detect cooperation for self-tolerance between Aire and Fezf2, the latter of which unexpectedly

*Correspondence: yousuke.takahama@nih.gov.

AUTHOR CONTRIBUTIONS

A.U. and M.M.-L. performed the experiments, validated the results, analyzed the data, and wrote the manuscript. F.K.-Y. and A.S. performed the experiments. N.I. analyzed the pathological data. M.C.K. conducted single-cell RNA sequencing analysis. A.A. analyzed single-cell RNA sequencing data. Y.T. conceived the study, supervised the research, and wrote the manuscript.

DECLARATION OF INTERESTS

The authors declare no competing interests.

SUPPLEMENTAL INFORMATION

Supplemental information can be found online at https://doi.org/10.1016/j.celrep.2024.114072.

regulates thymic tuft cells. Our results indicate an indispensable interplay among functionally diverse mTECs for the establishment of central self-tolerance.

Graphical Abstract

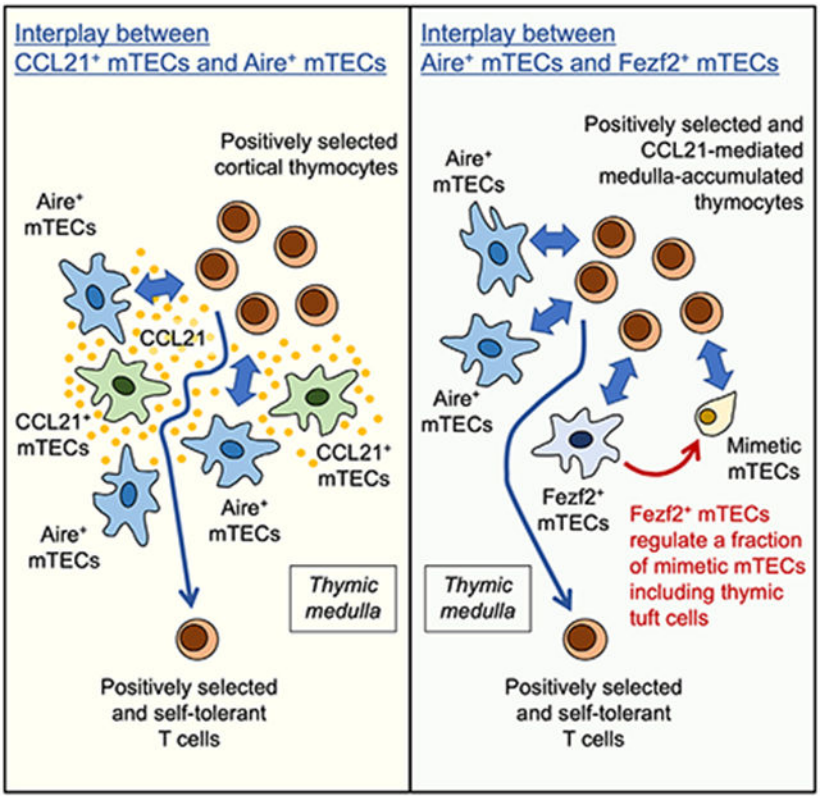

In brief

Ushio et al. show that functionally diverse medullary thymic epithelial cell (mTEC) subpopulations cooperate to prevent autoimmune pathology. The results demonstrate the interplay between diverse mTEC subpopulations, namely between CCL21^{+} mTECs and Aire^{+} mTECs and between Aire^{+} mTECs and Fezf2^{+} mTECs, for optimizing central tolerance.

INTRODUCTION

Medullary thymic epithelial cells (mTECs) essentially contribute to the establishment of central self-tolerance in T cells. Promiscuous gene expression by a major histocompatibility complex (MHC) class II^{high} CD80^{high} subpopulation of mTECs, termed mTEC^{high}, enables the transcription of a large spectrum of genes encoded by the self-genome.[1,2] The nuclear protein Aire plays a key role in the promiscuous gene expression by mTEC^{high} through the regulation of chromatin accessibility.[3,4] The non-redundant role of the transcription factor Fezf2 in supporting the promiscuous expression of Aire-independent genes by mTEC^{high} cells has been documented.[5,6] A variety of cellular mimeses in MHC class II^{low} CD80^{low} mTECs (mTEC^{low}) further contribute to providing additional self-antigens in the thymic medulla by forming a mosaic of various cell types in a tissue-specific and transcription

factor-dependent manner, including Pou2f3-dependent tuft cells and Hnf4α-dependent microfold cells.[7,8]

In addition to these self-antigen-displaying mTECs, an mTEC^{low} subpopulation produces the chemokine CCL21, which attracts developing thymocytes from the thymic cortex to the medulla.[9] Newly generated thymocytes in the thymic cortex are induced by T cell receptor (TCR) signals to express the chemokine receptor CCR7, a functional receptor for CCL21, so that TCR-engaged and positively selected thymocytes are attracted to migrate from the cortex to the medulla.[10] Unlike human and many mammalian genomes, in which CCL21 is encoded by a single gene, two molecular species, CCL21Ser and CCL21Leu, having one amino acid difference, are encoded in the mouse genome.[11,12] However, mTECs in the mouse predominantly express CCL21Ser encoded by the *Ccl21a* locus.[13] Accordingly, in mice lacking either CCR7 or CCL21Ser, positively selected mature thymocytes fail to accumulate in the medullary region, and, as a result, T cells fail to establish self-tolerance.[13-15] Another CCR7 ligand, CCL19, has no detectable role in the cortex-to-medulla migration of developing thymocytes.[13,16] Thus, CCL21-expressing mTECs represent a functional mTEC subset that attracts developing thymocytes for the establishment of self-tolerance.

Consequently, multiple subsets of functionally diverse mTECs contribute to self-tolerance in T cells. The self-antigen-displaying mTEC subset includes Aire$^+$ cells, Fezf2$^+$ cells, and a variety of thymic mimetic cells, whereas the thymocyte-attracting mTEC subset includes CCL21$^+$ cells. The self-antigen-displaying mTEC subset including Aire$^+$ cells is well appreciated to play an essential role in thymic medulla-dependent central self-tolerance, whereas the thymocyte-attracting CCL21$^+$ mTECs are viewed to support the interaction between self-antigen-displaying mTECs and developing thymocytes to facilitate self-tolerance in T cells. However, it is unclear whether and how these different mTEC subsets coordinate to establish thymic self-tolerance. In the present study, we show that double deficiency of Aire$^+$ mTECs and CCL21$^+$ mTECs in mice causes a far more severe autoimmune phenotype than single deficiency of either Aire$^+$ mTECs or CCL21$^+$ mTECs. Mice carrying a thymus lacking both Aire and CCL21 develop severe autoimmune inflammation equivalent to mice completely lacking functional mTECs. Aire and CCL21 synergize to optimize the negative selection of self-reactive thymocytes and regulatory T (Treg) cell generation in the thymus. These results indicate that Aire$^+$ mTECs and CCL21$^+$ mTECs non-redundantly cooperate to establish self-tolerance, preventing autoimmune disease. Our results also indicate that the coordination between Aire$^+$ mTECs and CCL21$^+$ mTECs is essential and sufficient to fulfill the function of the thymic medullary epithelium in the establishment of self-tolerance in T cells. We further provide results showing that Fezf2 unexpectedly regulates Pou2f3-dependent thymic tuft cells in the thymic medulla and cooperates with Aire to direct self-tolerance. These results demonstrate an indispensable interplay between functionally diverse mTEC subsets, most notably between self-antigen-displaying mTECs and thymocyte-attracting mTECs, for the establishment of central self-tolerance.

RESULTS

Tissue damage in mice deficient in Aire and CCL21

Thymocyte-attracting CCL21-producing mTECs, which are detectable by the expression of tandem dimer Tomato (tdTomato) fluorescent proteins in *Ccl21a*^{tdTomato} knockin mice[13] and intracellular CCL21 proteins in wild-type mice,[17] are largely distinct from self-antigen-displaying Aire^{+} mTECs (Figures S1A-S1C). To begin analyzing how these functionally distinct mTEC subsets contribute to central self-tolerance in the thymus, we first examined the onset of tissue lesions in Aire-deficient (Aire knockout [KO]) mice, CCL21-deficient (CCL21- KO) mice, and Aire/CCL21 double-deficient (Aire/CCL21 double knockout [DKO]) mice in the C57BL/6 genetic background.

As reported previously, Aire-KO mice exhibited a high penetrance of severe lymphocyte infiltration around the duct in the lacrimal and salivary glands (Figures 1A and 1B). Lymphocyte infiltration in the lacrimal and salivary glands was reproducibly detected at a high penetrance by 20 weeks of age in either male mice or female mice from two independently generated Aire-KO mouse lines[3,18] (Figures 1B and S2). Lymphocyte infiltration in the retina, lungs, pancreas, liver, and kidneys was also detectable, albeit at a low penetrance (Figures 1A-1C, and S2). The severe lymphocyte infiltration with tissue damage in the lacrimal glands was accompanied by a significantly reduced tear volume in Aire-KO mice (Figure 2A).

Mice deficient in CCL21Ser, which lacked CCL21 proteins in the thymus[13] and are hereafter called CCL21-KO mice, exhibited a spectrum of lymphocyte infiltration in a variety of tissues, similar to Aire-KO mice, at a high penetrance in the lacrimal and salivary glands and a low penetrance in the lungs, pancreas, liver, and kidneys (Figures 1A, 1B, and S2). Similar to Aire-KO mice, a reduction in tear volume was detected in CCL21-KO mice (Figure 2A). In contrast to Aire-KO mice, however, lymphocyte infiltration in the retina was not detectable in CCL21-KO mice (Figures 1A, 1B, and S2). Thus, in agreement with previous studies,[3,13] Aire-KO mice and CCL21-KO mice developed lesions in a variety of tissues in a similar but not identical spectrum. Tissue damage in the lacrimal glands coincided with reduced tear secretion in mice deficient in either Aire or CCL21. A recent study reported that embryonic CCL21^{+} mTECs include developmental potential to give rise to Aire^{+} mTECs.[19] Nonetheless, the number of Aire^{+} mTECs was not reduced in CCL21-KO mice (Figure S1D), indicating that tissue damage in CCL21-KO mice is not due to the reduction in the number of Aire^{+} mTECs.

To better understand how Aire and CCL21 contribute to the prevention of tissue damage, we next examined the pathology of Aire/CCL21-DKO mice. Notably, we found that Aire/CCL21-DKO mice exhibited severe lymphocyte infiltration at a high penetrance in many organs, including the retina, lungs, liver, and kidneys, as well as the lacrimal and salivary glands (Figures 1A, 1B, and 1C). The infiltrated lymphocytes indeed included CD3^{+} T cells (Figure S1E). In addition to the high penetrance in damage of many tissues, tissue lesions in Aire/CCL21-DKO mice were detected earlier in ontogeny and more severe in inflammation than the lesions in Aire-KO or CCL21-KO mice (Figures 1A-1C and S2). This was confirmed by the examination of inflammation foci around vessels in the lungs and

liver (Figures 2B and 2C). Tear volume reduction due to tissue damage was more severe in Aire/CCL21-DKO mice than in Aire-KO or CCL21-KO mice (Figure 2A). Damage in the liver of Aire/ CCL21-DKO mice was evident from an elevated leakage of the liver enzyme aspartate aminotransferase (AST) into the blood (Figure 2D) and splenomegaly associated with circulatory disturbance in the liver[20] (Figure 2E). These results indicate that Aire/CCL21-DKO mice exhibit far more severe damage in a variety of tissues than Aire-KO or CCL21-KO mice.

Autoimmune disease in mice deficient in Aire and CCL21 specifically in thymus epithelium

Aire and CCL21 in the thymus are specifically expressed in mTECs,[2,13] within largely distinct mTEC subpopulations (Figure S1C).[17] However, because the expression of Aire and CCL21 is not limited to the thymus,[21-24] tissue damage in mice deficient in Aire and/or CCL21 may have been affected by, or potentially due to, extrathymically expressed Aire and/or CCL21 in mice. To examine how Aire and CCL21 in mTECs specifically contribute to tissue damage prevention, we transplanted non-hematopoietic thymic stroma including mTECs[25] into athymic nude mice to reconstitute T cell development in the thymus microenvironment that lacks Aire and/or CCL21 (Figures 3A and 3B). T cell reconstitution was verified by the analysis of spleen cells 6 weeks after thymus transplantation (Figure S3).

As a result of this thymic stroma transplantation, we were able to readily detect severe autoimmune inflammation in the liver of B6-nude mice reconstituted with RelB-deficient (RelB-KO) thymus but not control B6 wild-type (WT) thymus (Figures 3C and 3D), in agreement with previous results.[26] RelB is a transcription factor that is essential for early mTEC development, and lack of RelB in the thymus stroma results in the formation of a thymus microenvironment that lacks functional mTECs and, therefore, onset of autoimmunity due to failure of establishment of thymic medulla-mediated central tolerance in T cells.[27-29]

Under the experimental condition of thymic stroma transplantation, we examined how T cell central tolerance is affected in the thymus microenvironment lacking Aire and/or CCL21. Because Aire and CCL21 in the thymus are specifically expressed in mTECs,[2,13] the loss of Aire and/or CCL21 in the thymic stroma reflects the specific deficiency of Aire and/or CCL21 in mTECs. We found that Aire deficiency specifically in mTECs is sufficient to cause autoimmune inflammation in the liver and lungs (Figures 3C, 3D, S4A, and S4B). We also found that CCL21 deficiency specifically in mTECs induced mild lymphocyte infiltration in the lungs and kidneys as well as in the salivary glands (Figure S4A-S4D). Compared with the inflammation caused by the Aire-deficient thymus, that caused by the CCL21-deficient thymus was less severe in the liver (Figures 3C and 3D). Thus, the deficiency of either Aire or CCL21 in mTECs causes a similar severity of autoimmune tissue damage in an overlapping, but not identical, spectrum of organs.

Importantly, Aire/CCL21-DKO thymus transplantation in athymic mice caused severe liver inflammation (Figures 3C and 3D). The liver damage in mice transplanted with the thymus deficient in both Aire and CCL21 was significantly more severe than that in mice transplanted with the thymus lacking either Aire or CCL21 (Figures 3C and 3D). Similarly, the inflammation in the lungs was significantly more severe in mice transplanted with

the Aire/CCL21-DKO thymus than in those transplanted with the Aire-KO or CCL21-KO thymus (Figures S4A and S4B). Mice transplanted with the Aire/CCL21-DKO thymus further exhibited inflammatory lesions in the salivary glands and kidneys (Figures S4C and S4D). Most strikingly, the tissue lesions caused by the transplantation of the Aire/CCL21-DKO thymus were comparable with those caused by the transplantation of the RelB-deficient thymus (Figures 3C and 3D). These results indicate that the thymus lacking both $Aire^+$ mTECs and $CCL21^+$ mTECs causes severe autoimmune tissue damage in mice, and the damage is equivalent in severity to that caused by the RelB-deficient thymus, which entirely lacks functional mTECs, and much more severe than that caused by the thymus that lacks either $Aire^+$ or $CCL21^+$ mTECs.

Collectively, these results indicate that $Aire^+$ mTECs and $CCL21^+$ mTECs individually and differently contribute to the prevention of autoimmune tissue damage. Importantly, however, the results show that the loss of both $Aire^+$ mTECs and $CCL21^+$ mTECs causes a more severe autoimmune disease than the loss of either $Aire^+$ or $CCL21^+$ mTECs, indicating that $Aire^+$ mTECs and $CCL21^+$ mTECs cooperate to establish thymic medulla-mediated central self-tolerance. The comparable severity in tissue damage between Aire/CCL21-DKO thymus-transplanted mice and RelB-deficient thymus-transplanted mice further indicates that the combination of $Aire^+$ mTECs and $CCL21^+$ mTECs is functionally equivalent to RelB-dependent entire mTECs in preventing autoimmune tissue damage in mice.

Negative selection in thymus deficient in Aire and CCL21

It is possible that $Aire^+$ mTECs and $CCL21^+$ mTECs cooperatively prevent autoimmune disease by supporting the negative selection of self-reactive T cells in the thymus. To examine whether the loss of $Aire^+$ mTECs and/or $CCL21^+$ mTECs affects the selection of self-reactive thymocytes, we analyzed the number of $TCR\beta^{high}$ $CD4^+CD8^-$ mature thymocytes that are reactive with two self-antigens, myelin oligodendrocyte glycoprotein (MOG) and apolipoprotein B (ApoB) (Figure 4A). It has been reported that MOG and ApoB represent self-antigens that are expressed by mTECs in an Aire-dependent and an Aire-enhanced manner, respectively.[2,30,31] The total number of $TCR\beta^{high}$ $CD4^+CD8^-$ mature thymocytes was not significantly altered in mice in the presence or absence of Aire and/or CCL21 (Figure 4B). As reported previously,[32] the number of $TCR\beta^{high}$ $CD4^+CD8^-$ mature thymocytes reactive with $I\text{-}A^b$ molecules associated with MOG peptides was significantly larger in Aire-KO mice than in control B6 mice, reflecting a defect in the Aire-dependent negative selection of MOG-reactive $CD4^+CD8^-$ thymocytes in the Aire-KO thymus (Figure 4C). On the contrary, the number of $TCR\beta^{high}$ $CD4^+CD8^-$ mature thymocytes reactive with $I\text{-}A^b$ molecules associated with ApoB peptides was only slightly and not significantly elevated in Aire-KO mice compared with the number in control B6 mice (Figure 4D), in agreement with previous studies showing that the negative selection of ApoB-reactive $CD4^+CD8^-$ thymocytes was detected by the reduced but remaining ApoB expressed in the Aire-deficient thymus.[32,33]

Unlike Aire-KO mice, CCL21-KO mice showed no significant increase in the number of MOG-reactive or ApoB-reactive $TCR\beta^{high}$ $CD4^+CD8^-$ mature thymocytes in comparison with control B6 mice (Figures 4C and 4D), demonstrating that the loss of CCL21 alone

does not significantly perturb the negative selection of these self-reactive thymocytes. Remarkably, however, Aire/CCL21-DKO mice were significantly defective in the negative selection of both MOG-reactive and ApoB-reactive TCRβ^{high} CD4^{+}CD8^{-} mature thymocytes (Figures 4C and 4D). Indeed, the negative selection of ApoB-reactive TCRβ^{high} CD4^{+}CD8^{-} mature thymocytes in Aire/CCL21-DKO mice was more severely defective than that in Aire-KO or CCL21-KO mice (Figure 4D), indicating that Aire and CCL21 cooperate to facilitate the negative selection of self-reactive thymocytes. As Aire and CCL21 in the thymus are specifically expressed by Aire^{+} and CCL21+ mTEC subsets, these results demonstrate that Aire^{+} mTECs and CCL21^{+} mTECs cooperate to promote the negative selection of self-reactive thymocytes.

Treg cell generation in thymus deficient in Aire and CCL21

In addition to supporting the clonal elimination of self-reactive thymocytes, the thymic medulla provides a microenvironment that promotes the development of Treg cells to ensure self-tolerance in the immune system.[26] We next examined whether Aire and CCL21 affect Treg cell development in the thymus (Figure 5A). We found that the number of Foxp3^{+}CD25^{+} TCRβ^{high} CD4^{+}CD8^{-}Treg cells in the thymus was significantly reduced in Aire-KO mice compared with control B6 mice (Figures 5B and 5C), as reported previously.[34,35] In addition, the number of Treg cells in the thymus was significantly reduced in CCL21-KO mice (Figure 5C), a finding newly detected using B6-background mice. More importantly, the number of Treg cells was further reduced in Aire/CCL21-DKO mice in comparison with the number in Aire-KO or CCL21-KO mice (Figure 5C).

The intrathymic Treg cell pool comprises newly generated Treg cells and recirculating peripheral Treg cells,[36,37] and Aire and CCR7 have been reported to affect Treg cell recirculation to the thymus.[38,39] Indeed, the number of CD73^{high} Foxp3^{+}CD25^{+} TCRβ^{high} CD4^{+}CD8^{-} thymocytes, which were enriched with thymus-recirculating Treg cells,[40,41] was more severely reduced in Aire/CCL21-DKO mice than in either Aire-KO or CCL21-KO mice (Figures 5D and 5E). In contrast, the numbers of peripheral Foxp3^{+}CD25^{+} TCRβ^{high} CD4^{+}CD8^{-}Treg cells, which were largely CD73^{high} in the spleen (Figure 5D), were not altered in mice deficient in Aire and/or CCL21 (Figure 5F), suggesting that Aire and CCL21 cooperate to affect the recirculation of peripheral Treg cells to the thymus. In addition, the number of Foxp3^{+}CD25^{-} TCRβ^{high} CD4^{+}CD8^{-} thymocytes, which predominantly represent immediate precursor cells that give rise to Foxp3^{+}CD25^{+} TCRβ^{high} CD4^{+}CD8^{-}Treg cells,[42] was also most severely reduced in Aire/CCL21-DKO mice in comparison with the numbers in Aire-KO or CCL21-KO mice (Figure 5G), demonstrating that the intrathymic Treg cell development from the precursor cells is most severely defective in Aire/CCL21-DKO mice in comparison with that in Aire-KO or CCL21-KO mice. These results together indicate that Aire^{+} mTECs and CCL21^{+} mTECs cooperate to establish self-tolerance by optimizing the negative selection of self-reactive T cells and the development and recirculation of Treg cells in the thymus.

Fezf2 affects a variety of genes associated with mTECs, including thymic tuft cells

The results presented so far indicate that Aire^{+} mTECs and CCL21^{+} mTECs cooperate to establish T cell self-tolerance. Because Aire^{+} mTECs and CCL21^{+} mTECs are functionally

different and belong to distinct mTEC subpopulations, our results reveal the cooperation between functionally different mTEC subsets to direct self-tolerance in T cells. Nonetheless, functional diversity in mTECs is not limited to the heterogeneity of thymocyte-attracting mTECs and self-antigen-displaying mTECs. In this regard, we finally attempted to examine whether functional cooperation might be additionally detectable in other combinations of highly diverse mTEC subpopulations. Even within self-antigen-displaying mTECs, multiple mTEC subpopulations appear to complement each other to cover a variety of self-antigens encoded by the self-genome. We specifically examined whether Aire$^+$ mTECs and Fezf2$^+$ mTECs might cooperate to establish central tolerance, as it has been reported that the transcription factor Fezf2 is important for the complementary expression of Aire-independent self-antigen genes in mTECs and that the expression spectra of Fezf2 and Aire in mTEC subpopulations overlap[43] but are different from each other.[5,6,44]

We examined whether and how the deficiency in Fezf2 and Aire in mTECs caused autoimmune lesions in mice. Because systemic Fezf2-deficient mice are lethal by 4 weeks of age owing to defective brain development,[45] we analyzed Fezf2-floxed mice[46] bred with either Foxn1-Cre-transgenic mice[47] or β5t-iCre knockin mice[48] to delete the *Fezf2* gene specifically in TECs. The Foxn1-Cre transgene is specific for TECs and skin epithelial cells,[47] whereas β5t-iCre is specifically active in cortico-medullary bipotent TEC progenitors and cortical TECs (cTECs).[48] TEC-specific deletion of Fezf2 caused the loss of Fezf2 mRNAs and proteins in mTECs (Figures S5A-S5C). Single-cell RNA sequencing analysis confirmed the loss of *Fezf2* in TECs (Figures 6A and S6A), the majority of which overlapped with the Aire-expressing mTEC cluster (Figures 6B and 6C), and demonstrated that Fezf2 deletion in TECs did not abolish the expression of pan-TEC-associated *Epcam* and *Foxn1,* cTEC-associated *Psmb11* and *Prss16*, and mTEC-associated *Aire* and *Ccl21a* (Figures 6C and 6D). The proportions of TEC clusters (i.e., cTECs, CCL21 mTECs, Aire mTECs, and mimetic mTECs) were largely equivalent in the presence or absence of Fezf2 (Figure 6E), except for a slight increase in the mimetic mTEC cluster caused by the loss of Fezf2, as described further in the next paragraph. In agreement with previous findings,[5] however, the loss of Fezf2 coincided with the reduction in a variety of Fezf2-dependent self-antigen genes, including *Fabp9*, *Resp18*, *Smtnl1*, *Maoa*, *Csrnp3*, and *Ttr* (Figures 6F, S6A, and S6B). Fezf2 deficiency in TECs also resulted in the reduction of a fraction of Aire-dependent tissue-restricted self-antigen genes, including *Mpo* and *Ins2* (Figures S6A and S6C), but did not abrogate the expression of various Aire-dependent tissue-restricted self-antigen genes, including *Camk2b*, *S100a8*, *Pllp*, and *Csn1s2a* (Figures 6G, S6A, and S6D). These results support the possibility that Fezf2 promotes the expression of a fraction of various tissue-restricted self-antigen genes in mTECs.

Unexpectedly, we also noticed that the absence of Fezf2 in TECs brought about a severe reduction in the mTEC expression of *Pou2f3* and *Hnf4a* (Figures 6D, 6H, and S6A), genes that encode transcription factors for the development of mimetic mTECs (*Pou2f3* for tuft mTECs and *Hnf4a* for enterohepato mTECs).[8,49-51] The expression of other mimetic mTEC-associated genes, *Krt10* (associated with keratinocyte mTECs) and *Vil1* (associated with intestinal enterocyte mTECs), was also diminished by the loss of Fezf2 (Figures 6D, S6A, and S6E). Indeed, the number of DCLK1$^+$ thymic tuft cells, a Pou2f3-dependent mimetic mTEC subpopulation,[49,50] was reduced in the thymic medulla of TEC-specific,

Fezf2-deficient mice (Figure 6I). Importantly, however, the frequency of mimetic mTEC cluster cells (Figure 6E) within TECs was not reduced but, rather, slightly elevated by the loss of Fezf2 (4.4%–4.5% of total TECs in control mice compared with 7.7% in Foxn1-Cre-dependent Fezf2-deficient mice and 11.9% in β5t-iCre-dependent Fezf2-deficient mice), indicating that Fezf2 deletion in TECs does not entirely remove mimetic mTECs. Indeed, a fraction of mimetic mTEC-associated genes, including *Spib* and *Tnfaip2* (associated with microfold mTECs), were not reduced in Fezf2-deficient TECs (Figures S6A and S6E). In addition, some genes, such as *Lamp1* and *Ctsd* were elevated in the Aire$^+$ mTEC cluster of TEC-specific Fezf2-deficient mice (Figure 6D). These results indicate that Fezf2 in TECs positively and negatively influences the expression of various mTEC-associated genes, including mimetic cell-associated genes, demonstrating that, in addition to regulating Aire-independent self-antigen genes, Fezf2 affects a variety of genes relevant for mTEC function, including the development of tuft cell-mimetic mTECs.

Lymphocyte infiltration in mice deficient in Aire and Fezf2

Mice deficient in Fezf2 in TECs (Fezf2-TEC-KO) exhibited significant but moderate lymphocyte infiltration in the lacrimal glands (Figures 7A-7C), in agreement with the role of Fezf2 in mTEC-mediated self-tolerance.[5] However, no significant inflammation was detectable in other tissues, including the salivary glands, retina, lungs, liver, pancreas, or kidneys, examined in Fezf2-TEC-KO mice even at 20 weeks of age (Figures 7A-7C). Lymphocyte infiltration in the lacrimal glands of Fezf2-TEC-KO mice was less severe than that of Aire-deficient mice; the latter exhibited a high penetrance of severe lymphocyte infiltration in the lacrimal and salivary glands and a low penetrance of lymphocyte infiltration in the retina, lungs, pancreas, liver, and kidneys (Figures 1 and 7). Indeed, unlike Aire deficiency, Fezf2 deficiency in TECs caused neither tear volume reduction nor lymphocyte infiltration in the lacrimal glands of mice at 10 weeks of age (Figures S7A and S7B). Importantly, we found that lymphocyte infiltration in the retina and lungs was slightly but significantly more severe in mice deficient in Aire- and TEC-specific Fezf2 (Aire-KO/Fezf2-TEC-KO) than in Aire-KO mice or Fezf2-TEC-KO mice (Figures 7C and 7D). Lymphocyte infiltration in other tissues, including the lacrimal and salivary glands, pancreas, liver, and kidneys, was equivalent and not significantly different between Aire-KO/Fezf2-TEC-KO mice and Aire-KO mice (Figures 7B and 7C). The number of Treg cells in the thymus was comparably reduced in Aire-KO mice and Aire-KO/Fezf2-TEC-DKO mice, whereas Fezf2-TEC-KO mice had a normal number of thymic Treg cells (Figure S7C), indicating that the number of thymic Treg cells is not altered by the loss of Fezf2 in the presence or absence of Aire. Thus, we detected a modest role of Fezf2 in TECs and a significant cooperation between Aire and Fezf2 to prevent autoimmune lesions, collectively indicating that Fezf2 has a role in mTECs to interplay with Aire to direct central self-tolerance.

DISCUSSION

The present results demonstrated two cases of interplay between different mTEC subpopulations for the establishment of self-tolerance: one between Aire$^+$ mTECs and CCL21$^+$ mTECs and the other between Aire$^+$ mTECs and Fezf2$^+$ mTECs. In particular,

we showed that Aire/CCL21-DKO mice develop far more severe tissue damage than mice deficient in either Aire or CCL21. The transplantation of non-hematopoietic thymic stroma into athymic nude mice reconfirmed that the thymus microenvironment that lacks both Aire and CCL21 causes severe autoimmune disease compared with the transplantation of the thymus lacking either Aire or CCL21. Because Aire and CCL21 in the thymus are expressed specifically in mTEC subpopulations, and because Aire-expressing mTECs and CCL21-expressing mTECs are largely distinct cellular populations, our results indicate that $Aire^+$ mTECs and $CCL21^+$ mTECs cooperate to direct central self-tolerance. Our results further revealed that, in comparison with Aire- or CCL21-single-KO mice, Aire/CCL21-DKO mice are highly defective in the mTEC-dependent negative selection of self-reactive T cells and the thymic development and recirculation of Treg cells. Collectively, our results indicate that $Aire^+$ mTECs and $CCL21^+$ mTECs coordinate to optimize negative selection and Treg cell generation in the thymus to prevent autoimmune disease, directing self-tolerance in T cells. Importantly, severe autoimmune lesions induced by the transplantation of an Aire/CCL21-DKO thymus were comparable with those provoked by transplantation of an RelB-deficient thymus entirely lacking mTECs, suggesting that the interplay between self-antigen-displaying mTECs and thymocyte-attracting mTECs is sufficient to fulfill the function of RelB-dependent thymic medullary epithelium in the establishment of self-tolerance in T cells.

Regarding the basis for the enhanced autoimmune phenotype in Aire/CCl21-DKO mice, it should be noted that Aire-expressing mTECs are mosaic in the expression of self-antigen genes, and a particular Aire-dependent self-antigen is displayed by only a small fraction (typically 1%–2%) of mature mTECs.[1,3,31] The CCL21-mediated medullary accumulation of developing thymocytes may promote efficient encounters between self-antigen-reactive thymocytes and relevant self-antigens expressed by a small fraction of Aire-dependent mTECs. The CCL21-mediated migration may also elevate the opportunity for self-antigen-reactive thymocytes to interact with Aire-independent self-antigens displayed in the thymic medulla. The enhanced autoimmune phenotype in Aire/CCl21-DKO mice additionally suggests that Aire-dependent self-tolerance in T cells may partially occur even without the CCL21-mediated medullary accumulation of developing thymocytes. For example, even without CCL21-dependent migration, self-reactive thymocytes may be able to interact with a small fraction of self-antigen-displaying Aire-expressing mTECs localized at the corticomedullary junction. Consequently, Aire and CCL21 cooperate to ensure self-tolerance in the thymus.

On the basis of our finding that $Aire^+$ mTECs and $CCL21^+$ mTECs cooperate to optimize thymic central tolerance, it is interesting to point out that different mTEC subsets are responsible for Aire-mediated self-antigen display and CCL21-mediated thymocyte attraction rather than a single mTEC subset mediating these two different functions. Importantly, the strength and kinetics of TCR signals determine the fate of developing T cells,[52,53] and the CCL21-CCR7 axis of chemokine signals modulates TCR signals when provided by antigen-presenting cells as co-stimulatory signals.[54,55] In the context of central tolerance in the thymic medulla, the TCR signal-mediated cell fate must be highly faithful to TCR engagement by self-antigen ligands provided by medullary self-antigen-presenting cells, including mTECs. The CCL21-mediated co-stimulatory modulation of TCR signals

may alter the threshold for T cell tolerance to medullary self-antigens, should CCR7 signals be provided by the same antigen-presenting cells. Consequently, the CCL21-mediated medullary attraction of positively selected thymocytes may need to be provided by an mTEC subset that is distinct from the self-antigen-displaying mTEC subset, which primarily interacts with positively selected thymocytes to accurately inspect the self-reactivity of developing T cells.

Our results showing the interplay between CCL21$^+$ mTECs and Aire$^+$ mTECs further suggest that CCL21$^+$ thymocyte-attracting mTECs may cooperate with other self-antigen-displaying mTECs, including self-mimetic mTECs. It is further interesting to speculate that the division of labor and the mutual interplay between functionally distinct mTEC subpopulations may not be limited to providing self-tolerance to newly generated αβ T cells. Indeed, the thymic medulla provides a microenvironment for the development of innate lymphocytes, including invariant natural killer (NK) T cells and γδ T cells.[56,57] Hematopoietic immune cell-attracting mTECs, which are not limited to CCL21-expressing mTECs but include other chemokine-expressing mTECs,[18,58,59] may cooperate with other mTEC subpopulations for the development of innate lymphocytes in the thymic medulla.

Our results also demonstrated the modest cooperation between Aire and Fezf2 in mTECs, in part supporting the previously reported role of Fezf2 in self-tolerance.[5,44] On the basis of previous results showing that Aire$^+$ mTECs and Fezf2$^+$ mTECs overlap but are not identical,[5] our results offer further support for the cooperation between diverse mTEC subpopulations to optimize central tolerance. Our results also support the previously described role of Fezf2 in regulating the expression of Aire-independent peripheral tissue-restricted self-antigens in mTECs.[5,44] Unexpectedly, our results further demonstrated that Fezf2 in mTECs affects the expression of a variety of genes, including *Pou2f3* and *Hnf4a*, which encode transcription factors important for the development of mimetic mTEC subpopulations.[8,49-51] Indeed, we detected a reduction in the number of DCLK1$^+$ thymic tuft cells, a prototypic cell subpopulation of mimetic mTECs,[49,50] in the thymus of TEC-specific, Fezf2-deficient mice. Fezf2 also negatively affects *Lamp1* and *Ctsd*, encoding the lysosomal-associated membrane protein LAMP1 and lysosomal protease cathepsin D, respectively, which are potentially important for self-antigen processing in mTECs. Thus, it is conceivable that Fezf2 in TECs influences the expression of a variety of genes relevant to mTEC function, including the development of a fraction of mimetic mTECs, rather than specifically regulating the expression of Aire-independent self-antigen genes.

Like Aire-deficient mice, TEC-specific Fezf2-deficient mice exhibited lymphocyte infiltration in the lacrimal glands, although we did not detect damage in any other tissues in TEC-specific, Fezf2-deficient mice. It is possible that certain lacrimal genes are regulated in an overlapping manner between Aire and Fezf2 in mTECs. We failed to detect an obvious Fezf2 regulation in mTECs of previously described lacrimal autoantigens, such as α-fodrin, encoded by *Sptan1*,[60] and odorant binding protein 1a, encoded by *Obp1a*.[61] However, *Klk1b16*, which encodes kalli-krein 1-related peptidase b16, detectable in the lacrimal glands,[62] is expressed in mTECs in a manner dependent on either Aire[31] or Fezf2.[5] Such genes, regulated in an overlapping manner between Aire and Fezf2, may in part explain the similarity in lacrimal inflammation between Aire-KO mice and Fezf2-TEC-KO mice.

Our results also showed that Fezf2 regulates a fraction of mimetic mTECs, including thymic tuft cells. Most mimetic mTECs belong to the $mTEC^{low}$ subpopulation[8] and are likely inefficient in antigen presentation. However, self-antigens produced by mimetic mTECs may be transferred to and crosspresented by MHC^{high} thymic dendritic cells, which in turn contribute to T cell self-tolerance in the thymic medulla.[63,64] Indeed, we detected equivalent numbers of $CD11c^{+}$ dendritic cells in the thymus of Aire/CCL21-DKO mice and Aire-KO/Fezf2-TEC-KO mice. Dendritic cell-mediated antigen presentation may facilitate the interplay among diverse mTEC subpopulations for the establishment of central tolerance.

Based on our results showing the cooperation between $Aire^{+}$ mTECs and $CCL21^{+}$ mTECs and between $Aire^{+}$ mTECs and $Fezf2^{+}$ mTECs, it is interesting to speculate that the cooperation among highly diverse mTEC subpopulations may be further extended to other mTEC combinations; for example, between $CCL21^{+}$ mTECs and $Fezf2^{+}$ mTECs, additionally including mimetic mTECs.

In conclusion, the present study revealed the interplay between CCL21-expressing, thymocyte-attracting mTECs and Aire-expressing, self-antigen-displaying mTECs to establish central tolerance in the immune system. These functionally distinct mTEC subsets coordinate to optimize the negative selection of self-reactive T cells and the generation of Treg cells in the thymus. The division of labor among the highly diverse mTECs may contribute to faithfully directing central tolerance by selecting developing T cells on the basis of self-reactivity and may further reflect the functionally multitasking aspect of the thymus medulla beyond central tolerance. In addition, our results revealed modest cooperation between Aire and Fezf2 for establishing central self-tolerance, further supporting the interplay among mTEC subpopulations.

Limitations of the study

Our results describe autoimmune phenotypes in mice in the C57BL/6 genetic background housed in a specific pathogen-free environment. It is known that genetic background considerably affects the severity and tissue spectrum of autoimmune disease. For example, Aire deficiency causes lethal pancreatitis,[65] and the loss of CCR7 causes severe thyroiditis[66] in non-obese diabetic (NOD)-background mice. The microbial environment also affects the immune system, including the onset of autoimmunity.[67,68] It is important to consider these genetic and environmental impacts, in addition to mouse-human differences, in view of the relevance of our findings to human health and disease. It is also important to note that currently available techniques for single-cell TEC preparation, which use enzymatic digestion of the thymus, are profoundly limited in cell recovery. Conventional TEC preparation can only liberate approximately 1% of cTECs and approximately 10% of mTECs.[69-71] In addition, it remains unknown whether those liberated TECs faithfully represent diverse TEC subpopulations in the thymus *in situ*. Single-cell RNA sequencing analysis of TECs presented in this study and other published studies may be biased to represent only a small fraction of enzymatic digestion-resistant TECs.

STAR★METHODS

RESOURCE AVAILABILITY

Lead contact—Further information and requests for resources and reagents should be directed to and will be fulfilled by the lead contact, Yousuke Takahama (yousuke.takahama@nih.gov).

Materials availability—This study did not generate new unique reagents.

Data and code availability

- Single-cell RNA-seq data have been deposited at the NCBI Gene Expression Omnibus (GEO: GSE244501) and are publicly available as of the date of publication.
- This paper does not report original code.
- Any additional information required to reanalyze the data reported in this work paper is available from the lead contact upon request.

EXPERIMENTAL MODEL AND STUDY PARTICIPANT DETAILS

Mice—C57BL/6 (B6)-backcrossed mice deficient in Ccl21a[13] and/or Aire (originally produced by Dr. Georg Hollander, Aire-KO GH strain)[18] were maintained in our animal facility. B6 mice, B6-Aire-KO mice (originally donated by Dr. Christophe Benoist; Aire-KO CB strain),[3] B6-RelB-deficient mice (originally donated by Dr. David Lo),[28] and B6-nu/nu athymic mice were obtained from The Jackson Laboratory. B6-Fezf2-flox mice[46] were bred with B6-Foxn1-Cre-transgenic mice[47] or B6-β5t-iCre-knock-in mice[48] to produce TEC-specific Fezf2-deficient (Fezf2-TEC-KO) mice. Pou2f3-deficient B6-background mice were the gift from Dr. Keiko Abe.[72] The lack of Aire, CCL21, and Fezf2 in TECs in indicated KO mice was confirmed (Figures 6, S1, and S5). Aire/CCL21-double knockout (DKO) mice and Aire/Fezf2-DKO mice were bred in our facility. All mouse experiments were performed under consent by the Animal Care and Use Committee of the National Cancer Institute (ASP 21–431, ASP 21–432, and EIB-076-3). The age and sex of the mice used in the experiments are described in individual figures and their legends.

METHOD DETAILS

Thymus transplantation—Fetal thymus lobes isolated from embryonic day (E) 15.5 were cultured for 5 days on sponge-supported Nucleopore filters (Millipore) placed in RPMI 1640-based complete medium containing 1.35 mM 2-deoxyguanosine (dGuo). After washing with PBS, the dGuo-treated thymus lobes were grafted underneath the renal capsule. Fetal thymus transplant recipients were analyzed 6 weeks after transplantation. T cell reconstitution in athymic recipients was confirmed by the detection of CD4, CD8, and TCRβ expression in spleen cells (Figure S3).

Tear volume measurement—For tear volume measurement, mice were anesthetized with ketamine (60 mg/kg body weight) and xylazine (6 mg/kg body weight), and intraperitoneally administered pilocarpine (2.5 mg/kg body weight). Tear volume

was determined by measuring the length of Zone-Quick phenol red thread (Ayumi Pharmaceutical). Measurements were performed twice for 5 min each after pilocarpine stimulation, and the average length of individual mice was recorded.

Pathological examination—Tissues for histopathological analysis were fixed with 10% phosphate-buffered formalin (pH 7.2, Sigma), paraffin sections were stained with hematoxylin and eosin (Histoserve), and images were analyzed by Zeiss ZEN (Zeiss). Pathological score was determined as follows: a score 0 indicates no inflammation; 1 indicates slight inflammation with one to five foci, where each focus is composed of more than 20 mononuclear cells; 2 indicates moderate inflammation with more than five such foci but without significant parenchymal damage; and 3 indicates severe inflammation resulting from the degeneration of parenchymal tissue with lymphocyte infiltration.

Immunofluorescence analysis—Thymus tissues were fixed with 4% paraformaldehyde and sliced into 10-μm-thick sections. Thymus sections were stained with antibodies specific for Aire (5H12, eBioscience), CCL21 (AAM27, Bio-Rad Laboratories), Ly51 (6C3, BioLegend), and DCLK1 (rabbit polyclonal, abcam) followed by AlexaFluor-conjugated anti-IgG antibodies (Invitrogen). Paraffin sections fixed with 10% formalin solution were deparaffinized and stained with antibody specific for CD3ε (D4V8L, Cell Signaling Technology) followed by AlexaFluor-conjugated anti-IgG antibodies (Invitrogen). Images were visualized with NIS-Elements (Nikon) and analyzed with ImageJ software.

Flow cytometric analysis and cell sorting—For the analysis of thymic epithelial cells (TECs), thymuses were minced and digested with 1 unit/ml Liberase TM (Roche) in the presence of 0.01% DNase I recombinant (Roche). Cells were stained with antibodies specific for anti-mouse CD45 (30-F11, BD Horizon), EpCAM (G8.8, BioLegend), and Ly51 (6C3, Biolegend), and for reactivity with UEA-1 (Vector Laboratories). For the analysis of thymocytes, cells were stained with antibodies specific for anti-mouse CD8a (53–6.7, eBioscience), CD4 (RM4-5, eBioscience), TCRβ (H57-597, BioLegend), CD25 (PC61, BioLegend), and CD73 (TY/11.8, BioLegend). For the detection of intracellular Aire, CCL21, and Foxp3, cells were fixed and permeabilized using Foxp3/Transcription Factor Staining Buffer Set (eBioscience) in accordance with the manufacturer's protocol, and stained with antibodies against Aire (5H12, eBioscience), CCL21 (AAM27, Bio-Rad Laboratories), and Foxp3 (FJK-16s, eBioscience). Flow cytometric analysis was performed on BD LSR Fortessa (BD Biosciences). For the sorting of TECs, Percoll density gradient centrifugation and magnetic cell isolation were performed prior to cell surface staining. In brief, cells with three layers of Percoll density were centrifuged at 2700 rpm for 20 min, and low-density cells were collected. The cells were incubated with CD45 MicroBeads (Miltenyi Biotec) and CD45-negative cells were collected. Cell sorting was performed on BD FACSAria SORP (BD Bioscience). Data were analyzed by using the FlowJo FACS Analysis software (BD Biosciences).

Peptide-MHC class II tetramer binding assay—PE- and APC-labeled peptide: I-A^b tetramers were obtained from the NIH Tetramer Core Facility. Peptides used were pMOG 38–49 (GWYRSPFSRVVH) and pApoB 978–993 (TGAYSNASSTESASY).

Tetramer enrichment was performed following a previously described protocol.[76] Briefly, thymocytes were incubated with PE- and APC-labeled tetramers (10 nM each) for 1 h at room temperature, and tetramer-bound cells were magnetically enriched using EasySep PE- and APC-positive selection kit II (StemCell Technologies). Cells were stained with antibodies against CD90.2 (30-H12, BioLegend), CD11b (M1/70, eBioscience), CD11c (N418, eBioscience), NK1.1(PK136, eBioscience), B220 (RA-3-6B2, eBioscience), TCRβ, CD8, and CD4, and analyzed on a flow cytometer.

Aspartate aminotransferase measurement—Serum aspartate aminotransferase (AST) detection was performed in accordance with the instructions included in the Mouse AST SimpleStep ELISA Kit (#ab263882, Abcam). Optical density (O.D.) at 450 nm was measured by a SpectraMax iD3 plate reader (Molecular Devices).

Immunoblot analysis—Cell lysates in RIPA lysis buffer supplemented with protease inhibitors (Millipore Sigma) were clarified by centrifugation at 14,000 rpm at 4°C for 20 min. Protein concentration was measured with a BCA protein assay kit (Pierce). Total protein (100 μg) was denatured in SDS protein gel loading solution (Quality Biological) supplemented with 10 mM DTT at 95°C for 10 min. Equal amounts of total proteins were electrophoresed in 4–20% NuPAGE Tris-glycine gels (Thermo Fisher) at 150 V for 2 h. The gels were transferred to positively charged PVDF membranes at 20 V for 7min. The membranes were blocked with 5% (w/v) nonfat milk in TBST (25 mm Tris, 150 mm NaCl, 0.05% Tween 20, pH 7.2) and probed with either anti-Fezf2 antibody (clone F441, IBL, 1:1000) or anti-β-tubulin antibody (BT7R, Thermo Fisher, 1:1000) at 4°C overnight, followed by washing with TBST and incubation with horseradish peroxidase-conjugated anti-rabbit IgG antibody (1:2500) at room temperature for 1 h. Proteins were visualized with a chemiluminescent substrate (Thermo Fisher)

Quantitative RT-PCR analysis—Total cellular RNAs extracted from TECs were reverse-transcribed (RT) with PrimeScript RT Master Mix (Takara). Quantitative real-time PCR was performed using SYBR Premix Ex Taq (Takara) and QuantStudio 6 Flex Real-time PCR System (Applied Biosystems). Amplified products were confirmed to be single bands in gel electrophoresis. Gene expression values were normalized to those of the housekeeping gene.

Single cell RNA sequencing analysis—A single-cell suspension of enriched TECs was prepared from the thymus of 2-week-old Fezf2-TEC-KO mice. In brief, minced thymus tissues were digested with 1 unit/ml Liberase TM (Roche) in the presence of 0.01% recombinant DNase I for 20 min. TECs were enriched by Percoll density gradient centrifugation and CD45 MicroBeads (Miltenyi Biotech). Single-cell 3′ transcriptomic profiles were obtained with a 10× Genomics system. Barcodes filtration was done using miQC,[77] and individual sample normalization was done using SCTransform through Seurat V3.[73] Doublets were detected using DoubletFinder V2 with a doublet estimate of 3%. Data were integrated using the Seurat V4 Package with default using the CCA method[74] settings, clustering, dimension reduction and sample integration, clustered using the SLM algorithm and a resolution of 0.6, and projected using Uniform Manifold Approximation and Projection (UMAP)[75] with the top 50 principal components. Average gene expression per

cluster was calculated and clusters were annotated using SingleR[78] annotation and manual removal of cells expressing CD45-encoding *Ptprc* then using a resolution of 0.2 and top 30 PCs to reconstruct clustering and UMAP. Fezf2 deficiency was examined by the extraction of exon 2 reads from chr14 12345238-12344349 from the bam files and added to the count matrix. Single-cell RNA sequencing data are deposited in NCBI Gene Expression Omnibus (https://www.ncbi.nlm.nih.gov/geo) with the accession number GSE244501.

QUANTIFICATION AND STATISTICAL ANALYSIS

Statistical analysis was performed with one-way ANOVA with Tukey's multiple comparisons test using GraphPad Prism 8 and 9 (GraphPad Software).*p* values of 0.05 or lower were considered to denote significance. All values are means and SEMs, unless otherwise specified. The sample numbers (n) are indicated in figure legends.

Supplementary Material

Refer to Web version on PubMed Central for supplementary material.

ACKNOWLEDGMENTS

We thank Georg Hollander for Foxn1-Cre-transgenic mice, Nenad Sestan for Fezf2-flox mice, and Keiko Abe for Pou2f3-deficient mice; Masashi Watanabe for the peptide-MHC tetramer assay; Assiatu Crossman, Susan Sharrow, Larry Granger, and William Hajjar for flow cytometry analysis and cell sorting; Jan Wisniewski for microscopy analysis; Christine Perella, Jacqui Clem, Mandi Miller, Robert Sui Nawl, Jeffery Chiang, and Alison Jacques for mouse colony management; and Graham Anderson, Alfred Singer, Izumi Ohigashi, and Masashi Watanabe for reading the manuscript. This work was supported by the Intramural Research Program (ZIA BC 011806) of the National Institutes of Health, the National Cancer Institute, and the Center for Cancer Research.

REFERENCES

1. Derbinski J, Schulte A, Kyewski B, and Klein L (2001). Promiscuous gene expression in medullary thymic epithelial cells mirrors the peripheral self. Nat. Immunol 2, 1032–1039. 10.1038/ni723. [PubMed: 11600886]
2. Derbinski J, Gäbler J, Brors B,Tierling S, Jonnakuty S, Hergenhahn M, Peltonen L, Walter J, and Kyewski B (2005). Promiscuous gene expression in thymic epithelial cells is regulated at multiple levels. J.Exp. Med 202, 33–45. 10.1084/jem.20050471. [PubMed: 15983066]
3. Anderson MS, Venanzi ES, Klein L, Chen Z, Berzins SP, Turley SJ, von Boehmer H, Bronson R, Dierich A, Benoist C, and Mathis D (2002). Projection of an immunological self shadow within the thymus by the aire protein. Science 298, 1395–1401. 10.1126/science.1075958. [PubMed: 12376594]
4. Bansal K, Yoshida H, Benoist C, and Mathis D (2017). The transcriptional regulator Aire binds to and activates super-enhancers. Nat. Immunol 18, 263–273. 10.1038/ni.3675. [PubMed: 28135252]
5. Takaba H, Morishita Y, Tomofuji Y, Danks L, Nitta T, Komatsu N, Kodama T, and Takayanagi H (2015). Fezf2 orchestrates a thymic program of self-antigen expression for immune tolerance. Cell 163, 975–987. 10.1016/j.cell.2015.10.013. [PubMed: 26544942]
6. Tomofuji Y, Takaba H, Suzuki HI, Benlaribi R, Martinez CDP, Abe Y, Morishita Y, Okamura T, Taguchi A, Kodama T, and Takayanagi H (2020). Chd4 choreographs self-antigen expression for central immune tolerance. Nat. Immunol 21, 892–901. 10.1038/s41590-020-0717-2. [PubMed: 32601470]
7. Farr AG, Dooley JL, and Erickson M (2002). Organization of thymic medullary epithelial heterogeneity: implications for mechanisms of epithelial differentiation. Immunol. Rev 189, 20–27. 10.1034/j.1600-065x.2002.18903.x. [PubMed: 12445262]

8. Michelson DA, Hase K, Kaisho T, Benoist C, and Mathis D (2022). Thymic epithelial cells co-opt lineage-defining transcription factors to eliminate autoreactive T cells. Cell 185, 2542–2558.e18. 10.1016/j.cell.2022.05.018. [PubMed: 35714609]
9. Takahama Y, Ohigashi I, Baik S, and Anderson G (2017). Generation of diversity in thymic epithelial cells. Nat. Rev. Immunol 17, 295–305. 10.1038/nri.2017.12. [PubMed: 28317923]
10. Ueno T, Saito F, Gray DHD, Kuse S, Hieshima K, Nakano H, Kakiuchi T, Lipp M, Boyd RL, and Takahama Y (2004). CCR7 signals are essential for cortex-medulla migration of developing thymocytes. J. Exp. Med 200, 493–505. 10.1084/jem.20040643. [PubMed: 15302902]
11. Nakano H, and Gunn MD (2001). Gene duplications at the chemokine locus on mouse chromosome 4: multiple strain-specific haplotypes and the deletion of secondary lymphoid-organ chemokine and EBI-1 ligand chemokine genes in the *plt* mutation. J. Immunol 166, 361–369. 10.4049/jimmunol.166.1.361. [PubMed: 11123313]
12. Chen SC, Vassileva G, Kinsley D, Holzmann S, Manfra D, Wiekowski MT, Romani N, and Lira SA (2002). Ectopic expression of the murine chemokines CCL21a and CCL21b induces the formation of lymph node-like structures in pancreas, but not skin, of transgenic mice. J. Immunol 168, 1001–1008. 10.4049/jimmunol.168.3.1001. [PubMed: 11801632]
13. Kozai M, Kubo Y, Katakai T, Kondo H, Kiyonari H, Schaeuble K, Luther SA, Ishimaru N, Ohigashi I, and Takahama Y (2017). Essential role of CCL21 in establishment of central self-tolerance in T cells. J. Exp. Med 214, 1925–1935. 10.1084/jem.20161864. [PubMed: 28611158]
14. Kurobe H, Liu C, Ueno T, Saito F, Ohigashi I, Seach N, Arakaki R, Hayashi Y, Kitagawa T, Lipp M, et al. (2006). CCR7-dependent cortex-to-medulla migration of positively selected thymocytes is essential for establishing central tolerance. Immunity 24, 165–177. 10.1016/j.immuni.2005.12.011. [PubMed: 16473829]
15. Nitta T, Nitta S, Lei Y, Lipp M, and Takahama Y (2009). CCR7-mediated migration of developing thymocytes to the medulla is essential for negative selection to tissue-restricted antigens. Proc. Natl. Acad. Sci. USA 106, 17129–17133. 10.1073/pnas.0906956106. [PubMed: 19805112]
16. Link A, Vogt TK, Favre S, Britschgi MR, Acha-Orbea H, Hinz B, Cyster JG, and Luther SA (2007). Fibroblastic reticular cells in lymph nodes regulate the homeostasis of naive T cells. Nat. Immunol 8, 1255–1265. 10.1038/ni1513. [PubMed: 17893676]
17. Lkhagvasuren E, Sakata M, Ohigashi I, and Takahama Y (2013). Lymphotoxin β receptor regulates the development of CCL21-expressing subset of postnatal medullary thymic epithelial cells. J. Immunol 190, 5110–5117. 10.4049/jimmunol.1203203. [PubMed: 23585674]
18. Lei Y, Ripen AM, Ishimaru N, Ohigashi I, Nagasawa T, Jeker LT, Bösl MR, Holländer GA, Hayashi Y, Malefyt R.d.W., et al. (2011). Aire-dependent production of XCL1 mediates medullary accumulation of thymic dendritic cells and contributes to regulatory T cell development. J. Exp. Med 208, 383–394. 10.1084/jem.20102327. [PubMed: 21300913]
19. Ohigashi I, White AJ, Yang MT, Fujimori S, Tanaka Y, Jacques A, Kiyonari H, Matsushita Y, Turan S, Kelly MC, et al. (2024). Developmental conversion of thymocyte-attracting cells into self-antigen-displaying cells in embryonic thymus medulla epithelium. Elife 12, 92552. 10.7554/eLife.92552.
20. De Gottardi A, Sempoux C, and Berzigotti A (2022). Porto-sinusoidal vascular disorder. J. Hepatol 77, 1124–1135. 10.1016/j.jhep.2022.05.033. [PubMed: 35690264]
21. Gardner JM, Devoss JJ, Friedman RS, Wong DJ, Tan YX, Zhou X, Johannes KP, Su MA, Chang HY, Krummel MF, and Anderson MS (2008). Deletional tolerance mediated by extrathymic Aire-expressing cells. Science 321, 843–847. 10.1126/science.1159407. [PubMed: 18687966]
22. Dobeš J, Ben-Nun O, Binyamin A, Stoler-Barak L, Oftedal BE, Goldfarb Y, Kadouri N, Gruper Y, Givony T, Zalayat I, et al. (2022). Extrathymic expression of Aire controls the induction of effective T_H17 cell-mediated immune response to *Candida albicans*. Nat. Immunol 23, 1098–1108. 10.1038/s41590-022-01247-6. [PubMed: 35761088]
23. Gunn MD, Kyuwa S, Tam C, Kakiuchi T, Matsuzawa A, Williams LT , and Nakano H (1999). Mice lacking expression of secondary lymphoid organ chemokine have defects in lymphocyte homing and dendritic cell localization. J. Exp. Med 189,451–460. 10.1084/jem.189.3.451. [PubMed: 9927507]

24. Ngo VN, Cornall RJ, and Cyster JG (2001). Splenic T zone development is B cell dependent. J. Exp. Med 194, 1649–1660. 10.1084/jem.194.11.1649. [PubMed: 11733579]
25. Jenkinson EJ, Franchi LL, Kingston R, and Owen JJ (1982). Effect of deoxyguanosine on lymphopoiesis in the developing thymus rudiment in vitro: application in the production of chimeric thymus rudiments. Eur. J. Immunol 12, 583–587. 10.1002/eji.1830120710. [PubMed: 6126365]
26. Cowan JE, Parnell SM, Nakamura K, Caamano JH, Lane PJL, Jenkinson EJ, Jenkinson WE, and Anderson G (2013). The thymic medulla is required for Foxp3$^+$ regulatory but not conventional CD4$^+$ thymocyte development. J. Exp. Med 210, 675–681. 10.1084/jem.20122070. [PubMed: 23530124]
27. Weih F, Carrasco D, Durham SK, Barton DS, Rizzo CA, Ryseck RP, Lira SA, and Bravo R (1995). Multiorgan inflammation and hematopoietic abnormalities in mice with a targeted disruption of RelB, a member of the NF-kappa B/Rel family. Cell 80, 331–340. 10.1016/0092-8674(95)90416-6. [PubMed: 7834753]
28. Burkly L, Hession C, Ogata L, Reilly C, Marconi LA, Olson D, Tizard R, Cate R, and Lo D (1995). Expression of relB is required for the development of thymic medulla and dendritic cells. Nature 373, 531–536. 10.1038/373531a0. [PubMed: 7845467]
29. Riemann M, Andreas N, Fedoseeva M, Meier E, Weih D, Freytag H, Schmidt-Ullrich R, Klein U, Wang ZQ, and Weih F (2017). Central immune tolerance depends on crosstalk between the classical and alternative NF-κB pathways in medullary thymic epithelial cells. J. Autoimmun 81, 56–67. 10.1016/j.jaut.2017.03.007. [PubMed: 28385374]
30. Ko HJ, Kinkel SA, Hubert FX, Nasa Z, Chan J, Siatskas C, Hirubalan P,Toh BH, Scott HS, and Alderuccio F (2010).Transplantation of autoimmune regulator-encoding bone marrow cells delays the onset of experimental autoimmune encephalomyelitis. Eur. J. Immunol 40, 3499–3509. 10.1002/eji.201040679. [PubMed: 21108470]
31. Sansom SN, Shikama-Dorn N, Zhanybekova S, Nusspaumer G, Macaulay IC, Deadman ME, Heger A, Ponting CP, and Holländer GA (2014). Population and single-cell genomics reveal the Aire dependency, relief from Polycomb silencing, and distribution of self-antigen expression in thymic epithelia. Genome Res. 24, 1918–1931. 10.1101/gr.171645.113. [PubMed: 25224068]
32. Watanabe M, Lu Y, Breen M, and Hodes RJ (2020). B7-CD28 costimulation modulates central tolerance via thymic clonal deletion and Treg generation through distinct mechanisms. Nat. Commun 11, 6264. 10.1038/s41467-020-20070-x. [PubMed: 33293517]
33. Nettersheim FS, Braumann S, Kobiyama K, Orecchioni M, Vassallo M, Miller J, Ali A, Roy P, Saigusa R, Wolf D, et al. (2021). Autoimmune regulator (AIRE) deficiency does not affect atherosclerosis and CD4 T cell immune tolerance to apolipoprotein B. Front. Cardiovasc. Med 8, 812769. 10.3389/fcvm.2021.812769.
34. Aschenbrenner K, D'Cruz LM, Vollmann EH, Hinterberger M, Emmerich J, Swee LK, Rolink A, and Klein L (2007). Selection of Foxp3$^+$ regulatory T cells specific for self antigen expressed and presented by Aire$^+$ medullary thymic epithelial cells. Nat. Immunol 8, 351–358. 10.1038/ni1444. [PubMed: 17322887]
35. Abramson J, and Anderson G (2017). Thymic epithelial cells. Annu. Rev. Immunol 35, 85–118. 10.1146/annurev-immunol-051116-052320. [PubMed: 28226225]
36. Thiault N, Darrigues J, Adoue V, Gros M, Binet B, Perals C, Leobon B, Fazilleau N, Joffre OP, Robey EA, et al. (2015). Peripheral regulatory T lymphocytes recirculating to the thymus suppress the development of their precursors. Nat. Immunol 16, 628–634. 10.1038/ni.3150. [PubMed: 25939024]
37. Weist BM, Kurd N, Boussier J, Chan SW, and Robey EA (2015). Thymic regulatory T cell niche size is dictated by limiting IL-2 from antigen-bearing dendritic cells and feedback competition. Nat. Immunol 16, 635–641. 10.1038/ni.3171. [PubMed: 25939026]
38. Cowan JE, Baik S, McCarthy NI, Parnell SM, White AJ, Jenkinson WE, and Anderson G (2018). Aire controls the recirculation of murine Foxp3$^+$ regulatory T-cells back to the thymus. Eur. J. Immunol 48, 844–854. 10.1002/eji.201747375. [PubMed: 29285761]
39. Cowan JE, McCarthy NI, and Anderson G (2016). CCR7 Controls Thymus Recirculation, but Not Production and Emigration, of Foxp3$^+$ T Cells. Cell Rep. 14, 1041–1048. 10.1016/j.celrep.2016.01.003. [PubMed: 26832402]

40. Owen DL, Mahmud SA, Sjaastad LE, Williams JB, Spanier JA, Simeonov DR, Ruscher R, Huang W, Proekt I, Miller CN, et al. (2019). Thymic regulatory T cells arise via two distinct developmental programs. Nat. Immunol 20, 195–205. 10.1038/s41590-018-0289-6. [PubMed: 30643267]
41. Santamaria JC, Borelli A, and Irla M (2021). Regulatory T cell heterogeneity in the thymus: Impact on their functional activities. Front. Immunol 12, 643153. 10.3389/fimmu.2021.643153. [PubMed: 33643324]
42. Tai X, Indart A, Rojano M, Guo J, Apenes N, Kadakia T, Craveiro M, Alag A, Etzensperger R, Badr ME, et al. (2023). How autoreactive thymocytes differentiate into regulatory versus effector $CD4^+$ T cells after avoiding clonal deletion. Nat. Immunol 24, 637–651. 10.1038/s41590-023-01469-2. [PubMed: 36959291]
43. Cosway EJ, Lucas B, James KD, Parnell SM, Carvalho-Gaspar M, White AJ, Tumanov AV, Jenkinson WE, and Anderson G (2017). Redefining thymus medulla specialization for central tolerance. J. Exp. Med 214, 3183–3195. 10.1084/jem.20171000. [PubMed: 28830910]
44. Takaba H, and Takayanagi H (2017). The mechanisms of T cell selection in the thymus. Trends Immunol. 38, 805–816. 10.1016/j.it.2017.07.010. [PubMed: 28830733]
45. Hirata T, Suda Y, Nakao K, Narimatsu M, Hirano T, and Hibi M (2004). Zinc finger gene fez-like functions in the formation of subplate neurons and thalamocortical axons. Dev. Dynam 230, 546–556. 10.1002/dvdy.20068.
46. Han W, Kwan KY, Shim S, Lam MMS, Shin Y, Xu X, Zhu Y, Li M, and Sestan N(2011). TBR1 directly represses Fezf2 to control the laminar origin and development of the corticospinal tract. Proc. Natl. Acad. Sci. USA 108, 3041–3046. 10.1073/pnas.1016723108. [PubMed: 21285371]
47. Zuklys S, Gill J, Keller MP, Hauri-Hohl M, Zhanybekova S, Balciunaite G, Na KJ, Jeker LT, Hafen K, Tsukamoto N, et al. (2009). Stabilized beta-catenin in thymic epithelial cells blocks thymus development and function. J. Immunol 182, 2997–3007. 10.4049/jim-munol.0713723. [PubMed: 19234195]
48. Ohigashi I, Zuklys S, Sakata M, Mayer CE, Zhanybekova S, Murata S, Tanaka K, Holländer GA, and Takahama Y (2013). Aire-expressing thymic medullary epithelial cells originate from β5t-expressing progenitor cells. Proc. Natl. Acad. Sci. USA 110, 9885–9890. 10.1073/pnas.1301799110. [PubMed: 23720310]
49. Miller CN, Proekt I, von Moltke J, Wells KL, Rajpurkar AR, Wang H, Rattay K, Khan IS, Metzger TC, Pollack JL, et al. (2018). Thymic tuft cells promote an IL-4-enriched medulla and shape thymocyte development. Nature 559, 627–631. 10.1038/s41586-018-0345-2. [PubMed: 30022164]
50. Bornstein C, Nevo S, Giladi A, Kadouri N, Pouzolles M, Gerbe F, David E, Machado A, Chuprin A, Tóth B, et al. (2018). Single-cell mapping of the thymic stroma identifies IL-25-producing tuft epithelial cells. Nature 559, 622–626. 10.1038/s41586-018-0346-1. [PubMed: 30022162]
51. Michelson DA, Zuo C, Verzi M, Benoist C, and Mathis D (2023). Hnf4 activates mimetic-cell enhancers to recapitulate gut and liver development within the thymus. J. Exp. Med 220, e20230461. 10.1084/jem.20230461. [PubMed: 37399024]
52. Starr TK, Jameson SC, and Hogquist KA (2003). Positive and negative selection of T cells. Annu. Rev. Immunol 21, 139–176. 10.1146/annurev.immunol.21.120601.141107. [PubMed: 12414722]
53. Singer A, Adoro S, and Park JH (2008). Lineage fate and intense debate: myths, models and mechanisms of CD4- versus CD8-lineage choice. Nat. Rev. Immunol 8, 788–801. 10.1038/nri2416. [PubMed: 18802443]
54. Gollmer K, Asperti-Boursin F, Tanaka Y, Okkenhaug K, Vanhaesebroeck B, Peterson JR, Fukui Y, Donnadieu E, and Stein JV (2009). CCL21 mediates $CD4^+$ T-cell costimulation via a DOCK2/Rac-dependent pathway. Blood 114, 580–588. 10.1182/blood-2009-01-200923. [PubMed: 19451552]
55. Laufer JM, Kindinger I, Artinger M, Pauli A, and Legler DF (2018). CCR7 is recruited to the immunological synapse, acts as co-stimulatory molecule and drives LFA-1 clustering for efficient T cell adhesion through ZAP70. Front. Immunol 9, 3115. 10.3389/fimmu.2018.03115. [PubMed: 30692994]
56. White AJ, Jenkinson WE, Cowan JE, Parnell SM, Bacon A, Jones ND, Jenkinson EJ, and Anderson G (2014). An essential role for medullary thymic epithelial cells during the intrathymic

development of invariant NKT cells. J. Immunol 192, 2659–2666. 10.4049/jimmunol.1303057. [PubMed: 24510964]

57. Roberts NA, White AJ, Jenkinson WE, Turchinovich G, Nakamura K, Withers DR, McConnell FM, Desanti GE, Benezech C, Parnell SM, et al. (2012). Rank signaling links the development of invariant γδ T cell progenitors and Aire^{+} medullary epithelium. Immunity 36, 427–437. 10.1016/j.immuni.2012.01.016. [PubMed: 22425250]
58. Seach N, Ueno T, Fletcher AL, Lowen T, Mattesich M, Engwerda CR, Scott HS, Ware CF, Chidgey AP, Gray DHD, and Boyd RL (2008). The lymphotoxin pathway regulates Aire-independent expression of ectopic genes and chemokines in thymic stromal cells. J. Immunol 180, 5384–5392. 10.4049/jimmunol.180.8.5384. [PubMed: 18390720]
59. Lopes N, Charaix J, Cédile O, Sergé A, and Irla M (2018). Lymphotoxin ± fine-tunes T cell clonal deletion by regulating thymic entry of antigen-presenting cells. Nat. Commun 9, 1262. 10.1038/s41467-018-03619-9. [PubMed: 29593265]
60. Haneji N, Nakamura T, Takio K, Yanagi K, Higashiyama H, Saito I, Noji S, Sugino H, and Hayashi Y (1997). Identification of alpha-fodrin as a candidate autoantigen in primary Sjögren's syndrome. Science 276, 604–607. 10.1126/science.276.5312.604. [PubMed: 9110981]
61. DeVoss JJ, LeClair NP, Hou Y, Grewal NK, Johannes KP, Lu W, Yang T, Meagher C, Fong L, Strauss EC, and Anderson MS (2010). An autoimmune response to odorant binding protein 1a is associated with dry eye in the Aire-deficient mouse. J. Immunol 184, 4236–4246. 10.4049/jimmunol.0902434. [PubMed: 20237294]
62. Fava RA, Kennedy SM, Wood SG, Bolstad AI, Bienkowska J, Papandile A, Kelly JA, Mavragani CP, Gatumu M, Skarstein K, and Browning JL (2011). Lymphotoxin-beta receptor blockade reduces CXCL13 in lacrimal glands and improves corneal integrity in the NOD model of Sjögren's syndrome. Arthritis Res. Ther 13, R182. 10.1186/ar3507. [PubMed: 22044682]
63. Gallegos AM, and Bevan MJ (2004). Central tolerance to tissue-specific antigens mediated by direct and indirect antigen presentation. J. Exp. Med 200, 1039–1049. 10.1084/jem.20041457. [PubMed: 15492126]
64. Hubert FX, Kinkel SA, Davey GM, Phipson B, Mueller SN, Liston A, Proietto AI, Cannon PZF, Forehan S, Smyth GK, et al. (2011). Aire regulates the transfer of antigen from mTECs to dendritic cells for induction of thymic tolerance. Blood 118, 2462–2472. 10.1182/blood-2010-06-286393. [PubMed: 21505196]
65. Jiang W, Anderson MS, Bronson R, Mathis D, and Benoist C (2005). Modifier loci condition autoimmunity provoked by Aire deficiency. J. Exp. Med 202, 805–815. 10.1084/jem.20050693. [PubMed: 16172259]
66. Martin AP, Marinkovic T, Canasto-Chibuque C, Latif R, Unkeless JC, Davies TF, Takahama Y, Furtado GC, and Lira SA (2009). CCR7 deficiency in NOD mice leads to thyroiditis and primary hypothy-roidism. J. Immunol 183, 3073–3080. 10.4049/jimmunol.0900275. [PubMed: 19675158]
67. Beura LK, Hamilton SE, Bi K, Schenkel JM, Odumade OA, Casey KA, Thompson EA, Fraser KA, Rosato PC, Filali-Mouhim A, et al. (2016). Normalizing the environment recapitulates adult human immune traits in laboratory mice. Nature 532, 512–516. 10.1038/nature17655. [PubMed: 27096360]
68. Akagbosu B, Tayyebi Z, Shibu G, Paucar Iza YA, Deep D, Parisotto YF, Fisher L, Pasolli HA, Thevin V, Elmentaite R, et al. (2022). Novel antigen-presenting cell imparts Treg-dependent tolerance to gut microbiota. Nature 610, 752–760. 10.1038/s41586-022-05309-5. [PubMed: 36070798]
69. Sakata M, Ohigashi I, and Takahama Y (2018). Cellularity of thymic epithelial cells in the postnatal mouse. J. Immunol 200, 1382–1388. 10.4049/jimmunol.1701235. [PubMed: 29298829]
70. Hirakawa M, Nagakubo D, Kanzler B, Avilov S, Krauth B, Happe C, Swann JB, Nusser A, and Boehm T (2018). Fundamental parameters of the developing thymic epithelium in the mouse. Sci. Rep 8, 11095. 10.1038/s41598-018-29460-0. [PubMed: 30038304]
71. Venables T, Griffith AV, DeAraujo A, and Petrie HT (2019). Dynamic changes in epithelial cell morphology control thymic organ size during atrophy and regeneration. Nat. Commun 10, 4402. 10.1038/s41467-019-11879-2. [PubMed: 31562306]

72. Matsumoto I, Ohmoto M, Narukawa M, Yoshihara Y, and Abe K (2011). Skn-1a (Pou2f3) specifies taste receptor cell lineage. Nat. Neurosci 14, 685–687. 10.1038/nn.2820. [PubMed: 21572433]

73. Hafemeister C, and Satija R (2019). Normalization and variance stabilization of single-cell RNA-seq data using regularized negative binomial regression. Genome Biol. 20, 296. 10.1186/s13059-019-1874-1. [PubMed: 31870423]

74. Stuart T, Butler A, Hoffman P, Hafemeister C, Papalexi E, Mauck WM 3rd, Hao Y, Stoeckius M, Smibert P, and Satija R (2019). Comprehensive integration of single-cell data. Cell 177, 1888–1902.e21. 10.1016/j.cell.2019.05.031. [PubMed: 31178118]

75. Becht E, McInnes L, Healy J, Dutertre CA, Kwok IWH, Ng LG, Ginhoux F, and Newell EW (2018). Dimensionality reduction for visualizing single-cell data using UMAP. Nat. Biotechnol 37, 38–44. 10.1038/nbt.4314.

76. Chu HH, Moon JJ, Kruse AC, Pepper M, and Jenkins MK (2010). Negative selection and peptide chemistry determine the size of naive foreign peptide-MHC class II-specific $CD4^+$ T cell populations. J. Immunol 185, 4705–4713. 10.4049/jimmunol.1002276. [PubMed: 20861357]

77. Hippen AA, Falco MM, Weber LM, Erkan EP, Zhang K, Doherty JA, Vähärautio A, Greene CS, and Hicks SC (2021). miQC: An adaptive probabilistic framework for quality control of single-cell RNA-sequencing data. PLoS Comput. Biol 17, e1009290. 10.1371/journal.pcbi.1009290. [PubMed: 34428202]

78. Aran D, Looney AP, Liu L, Wu E, Fong V, Hsu A, Chak S, Naikawadi RP, Wolters PJ, Abate AR, et al. (2019). Reference-based analysis of lung single-cell sequencing reveals a transitional profibrotic macrophage. Nat. Immunol 20, 163–172. 10.1038/s41590-018-0276-y. [PubMed: 30643263]

Highlights

- Mice lacking CCL21^{+} mTECs and Aire^{+} mTECs exhibit a severe autoimmunity in C57BL/6 background
- CCL21^{+} mTECs and Aire^{+} mTECs cooperate for autoreactive T cell deletion and Treg cell generation
- Fezf2 has a modest but significant role in central tolerance in mice
- Fezf2 regulates a fraction of mimetic mTECs including thymic tuft cells

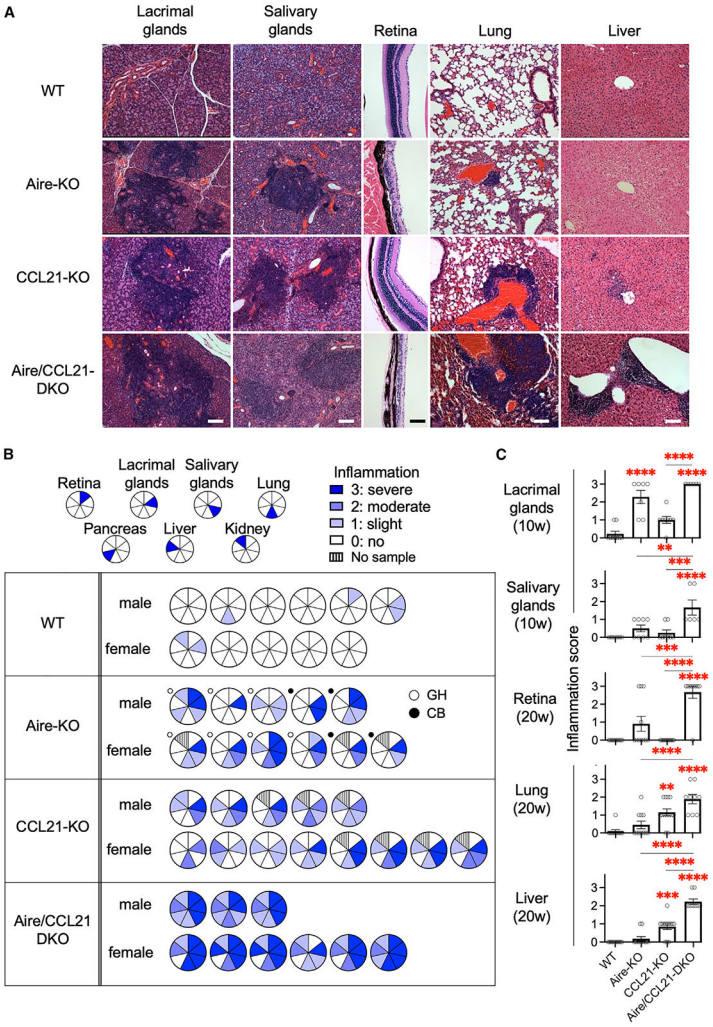

Figure 1. Tissue inflammation in mice deficient in Aire and/or CCL21

(A) Hematoxylin and eosin (H&E)-stained sections of the indicated tissues from female 20-week-old wild-type (WT), Aire knockout (KO), CCL21-KO, and Aire/ CCL21 double KO (DKO) mice. Representative data from at least 5 independent measurements ($n = 5–8$) are shown. Scale bars, 100 μm.

(B) Pie chart showing the inflammation score of the indicated tissues from the indicated mice at 20 weeks of age. Each pie chart shows the scores for one mouse. Open and closed circles in the Aire-KO group indicate the GH strain and CB stain, respectively, as described in the STAR Methods.

(C) Inflammation score of the indicated tissues from the indicated mice($n = 6–13$) in at least 5 independent measurements at 10 weeks of age (lacrimal glands and salivary glands) and 20 weeks of age (retina, lungs, and liver). Means ± SEMs are plotted. $^{**}p < 0.01$, $^{***}p < 0.001$, $^{****}p < 0.0001$.

See also Figures S1 and S2.

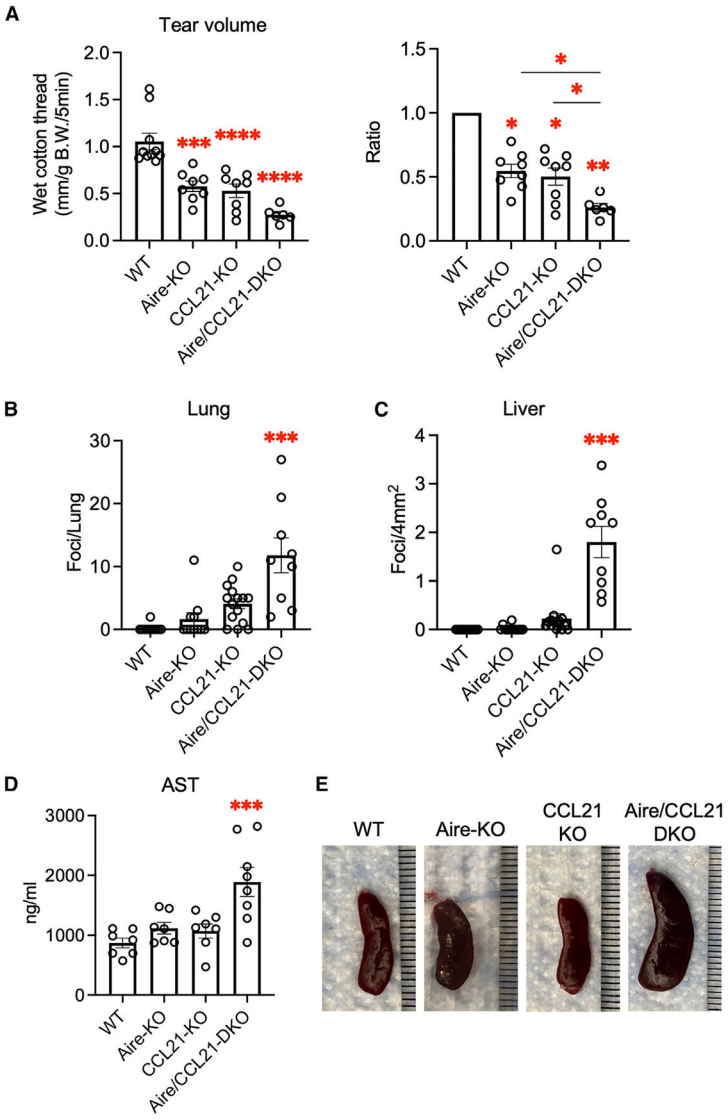

Figure 2. Tissue damage in mice deficient in Aire and/or CCL21

(A) Tear volume measured in the indicated mice. The length of cotton threads with absorbed tears was normalized to body weight (n = 6–8, 10–11 weeks old, 6 independent measurements). Plotted is mean ± SEM. ***$p < 0.001$, ****$p < 0.0001$.

(B and C) Numbers of inflammation foci in lung (B) and liver (C) sections.

(D) AST concentrations in serum of the indicated mice (n = 7–8, 20 weeks old, 2 independent measurements, mean ± SEM). ***$p < 0.001$.

(E) Representative macroscopic images of spleens from the indicated mice. Scale intervals indicate 1 mm.

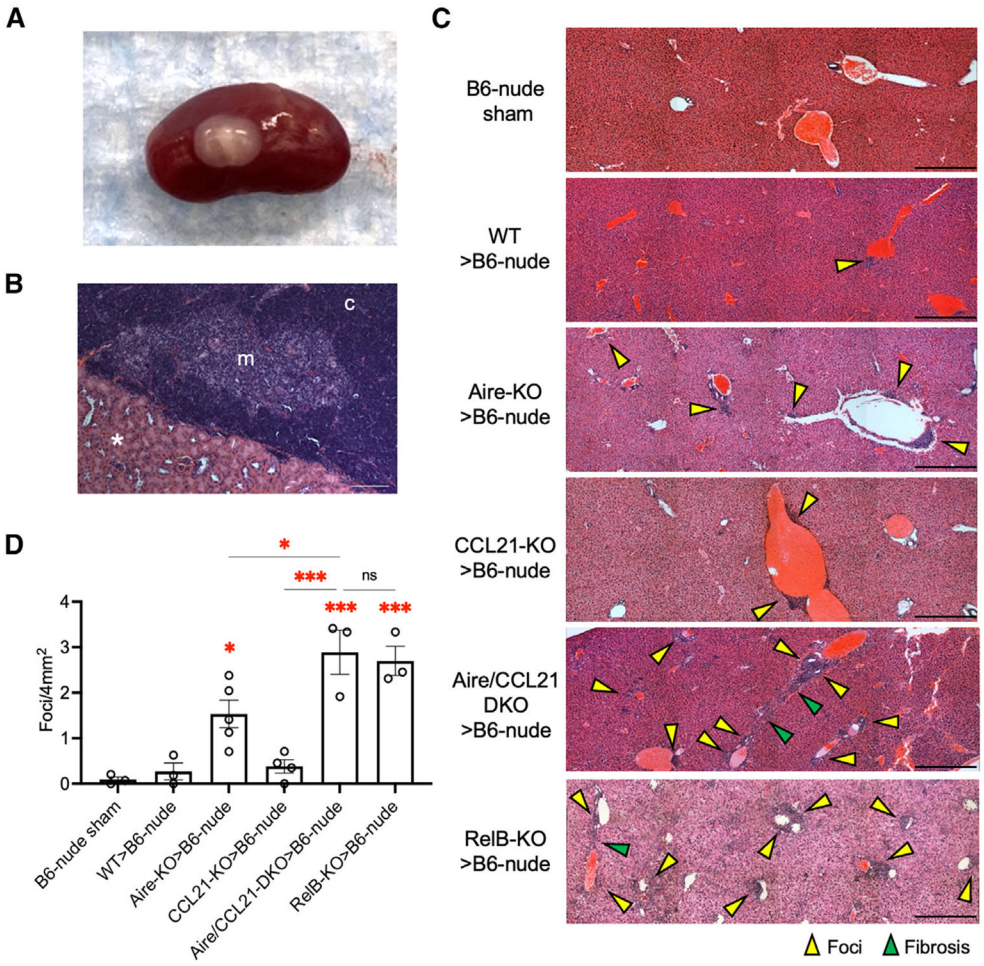

Figure 3. Tissues in athymic mice transplanted with a thymus deficient in Aire and/ or CCL21

(A and B) Kidney of a B6-nude mouse 6 weeks after thymus transplantation. Shown are a macroscopic image (A) and H&E-stained sections (B) of the transplanted thymus under the kidney capsule in B6-nude mice. c, cortex. m, medulla. *, kidney. Scale bar, 100 μm.

(C and D) H&E-stained liver sections from B6-nude mice transplanted with the thymus from the indicated mice. Sham operation mice received no thymus transplantation. Yellow arrowheads indicate foci, and green arrowheads indicate fibrosis (C). Representative data (n = 3–5) from 6 independent experiments are shown. Scale bars, 500 μm. Mean ± SEM of the number of foci per area (D) in the liver. *$p < 0.05$, ***$p < 0.001$; ns, not significant.

See also Figures S3 and S4.

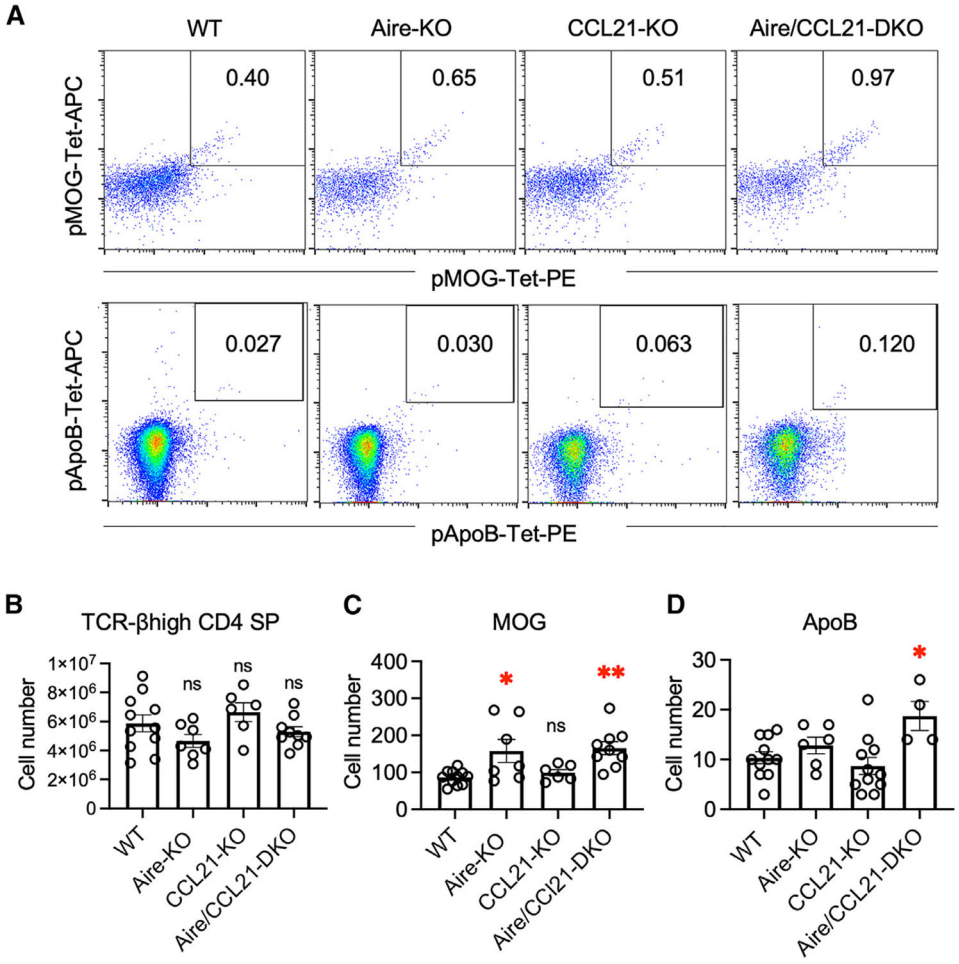

Figure 4. Negative selection of thymocytes in mice deficient in Aire and/or CCL21

(A) Representative flow cytometry profiles for the detection of pMOG-tetramer-binding cells (top) and pApoB-tetramer-binding cells (bottom) in TCRβ^{high} CD4 single-positive (SP) thymocytes (PI^{-}TCRβ^{high}CD4^{+}CD8−CD90.2 $^{+}$CD11b^{-}CD11c^{-}B220^{-}NK1.1−) from indicated mice. Numbers indicate the frequency of cells in the boxes.

(B–D) Numbers (means ± SEs) of TCRβ^{high} CD4 SP thymocytes (B), pMOG-tetramer-binding TCRβ^{high} CD4 SP thymocytes (n = 6–11 in 9 independent measurements) (C), and pApoB-tetramer-binding TCRβ^{high} CD4 SP thymocytes (n = 4–11 in 7 independent measurements) (D). Shown are data obtained from more than 5.0 × 10^{7} total thymocytes. *p < 0.05, **p < 0.01.

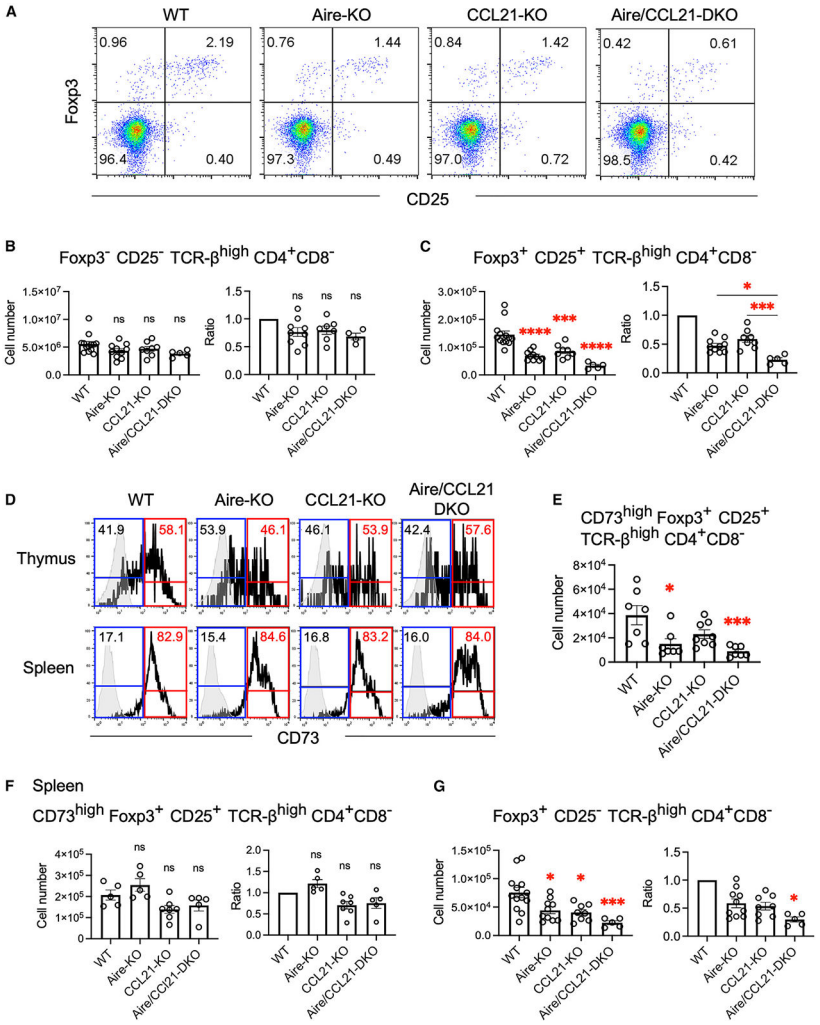

Figure 5. CD25$^+$ Foxp3$^+$ Treg cells in a thymus of mice deficient in Aire and/or CCL21

(A) Representative profiles for the detection of CD25$^+$Foxp3$^+$ Treg cells in TCRβ^{high} CD4 SP thymocytes from the indicated mice. Numbers indicate the frequency of cells in the boxes.

(B and C) Number (mean ± SE) of CD25$^-$Foxp3$^-$ TCRβ^{high} CD4 SP thymocytes (B) and CD25$^+$Foxp3$^+$TCRβ^{high} CD4 SP Treg cells (C) in the indicated mice (n = 5–13, 8–11 weeks, 6 independent experiments).

(D) Representative CD73 expression profiles of CD25$^+$Foxp3$^+$TCRβ^{high} CD4 SP Treg cells in the thymus and the spleen of the indicated mice. Numbers in boxes indicate frequencies of cells.

(E and F) Number (mean ± SE) of CD73$^+$CD25$^+$Foxp3$^+$TCRβ^{high} CD4 Treg cells in the thymus (n = 7–8,8–12 weeks, 4 independent experiments, E) and the spleen (n = 5–7, 8–12 weeks, 4 independent experiments, F).

(G) Number (mean ± SE) of CD25$^-$Foxp3$^+$ TCRβ^{high} CD4 SP Treg cell precursor thymocytes in the indicated mice (n = 5–13, 8–11 week, 6 independent experiments). Ratios of cell numbers in comparison with the numbers in control WT mice are also shown.

*p < 0.05, ***p < 0.001, ****p < 0.0001.

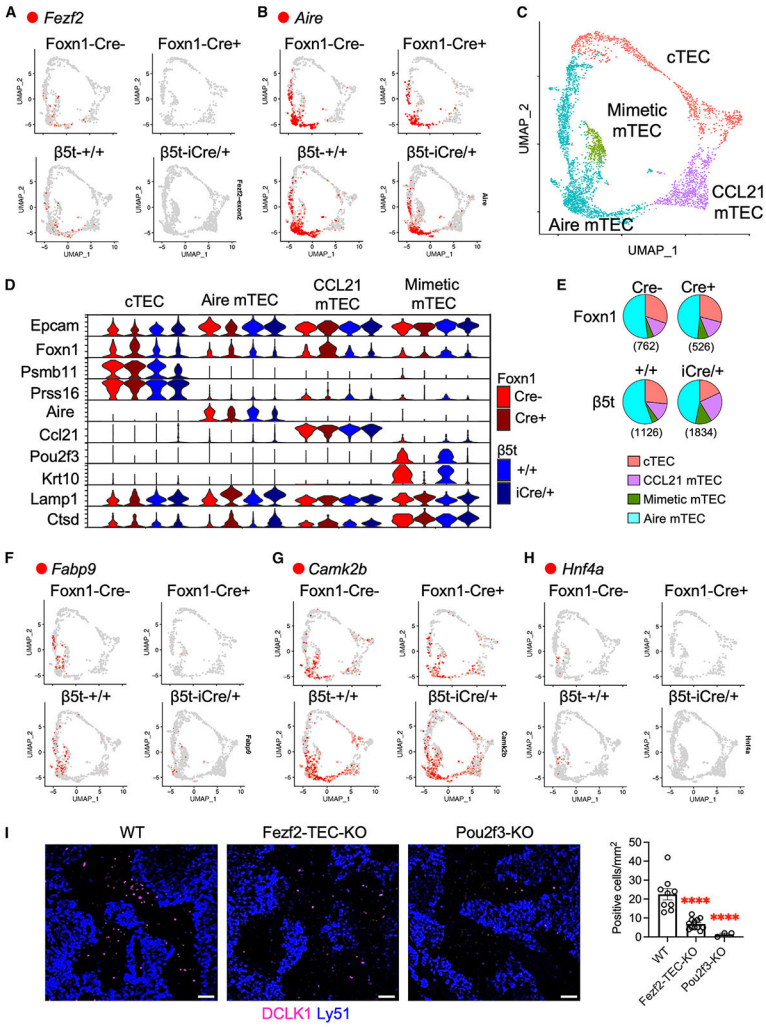

Figure 6. Single-cell RNA sequencing analysis in Fezf2-deficient TECs

(A and B) Uniform manifold approximation and projection (UMAP) profiles of *Fezf2* (A) and *Aire* (B) expression (red) in *Epcam*$^{+}$ *Cd45*$^{-}$ TECs (gray) isolated from the indicated mice.

(C and D) UMAP profile of *Epcam*$^{+}$ *Cd45*$^{-}$ TECs (C) reveals cell clusters as indicated based on gene expression profiles shown in violin plots (D). Equivalent expression of *Epcam* and *Foxn1* indicates that all 4 clusters are TECs (D). Selective expression of *Psmb11*, *Prss16*, *Aire*, *Ccl21a*, and *Pou2f3* (D) identifies the cTEC cluster, Aire^{+} mTEC cluster, CCL21^{+} mTEC cluster, and mimetic mTEC cluster (C). Mice analyzed were Fezf2$^{flox/flox}$ homozygotes in the absence or presence of the Foxn1-Cre-transgene and in the absence or presence of the β5t$^{iCre/+}$ heterozygous knockin allele (D). *Psmb11* encodes β5t, and the β5t-iCre allele carries the iCre sequence knocked in in place of the *Psmb11* sequence in the mouse genome.[48] Consequently, *Psmb11* transcripts in β5t$^{iCre/+}$ TECs were reduced to 51.6% of those in β5t$^{+/+}$ control mice ($p < 0.001$), whereas *Psmb11* transcripts in Foxn1-Cre^{+} TECs were 89.3% of those in Foxn1-Cre^{-} control mice (not statistically significant) (D). β5t$^{iCre/+}$ mice, in which *Psmb11* mRNA in cTECs is reduced to approximately half, did not show any reduction in β5t protein or its function.[48]

(E) Pie charts showing the proportions of the indicated clusters in *Epcam*$^{+}$ *Cd45*$^{-}$ TECs from the indicated mice. Numbers of total *Epcam*$^{+}$ *Cd45*$^{-}$ TECs in the indicated mice are shown in parentheses.

(F-H) UMAP profiles of the indicated genes (red).

(I) Immunofluorescence analysis of the thymus sections from Fezf2$^{flox/flox}$ control mice, β5t$^{iCre/+}$ Fezf2$^{flox/flox}$ TEC-specific Fezf2-deficient mice, and Pou2f3-deficient mice. DCLK1-expressing thymic tuft cells are detected in the Ly51^{-} medullary region in the thymus from control mice. Representative data from 3 individual measurements are shown. Scale bars, 250 μm. Plotted are the numbers of DCLK1^{+} cells in 1-mm^{2} areas in the thymus medulla, counted in 3 areas per mouse (n = 9).

See also Figures S5 and S6

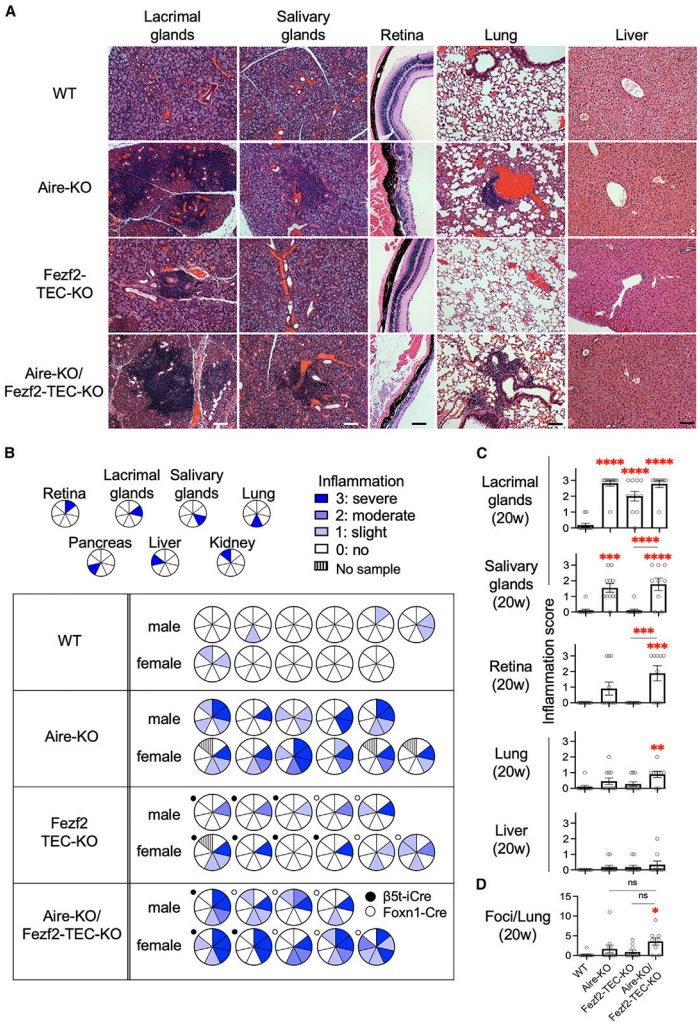

Figure 7. Lymphocyte infiltration in mice deficient in Aire and Fezf2

(A) H&E-stained sections of the indicated tissues from female 20-week-old WT; Aire KO; TEC-specific, Fezf2-deficient (Fezf2-TEC-KO); and Aire-KO/Fezf2-TEC-KO mice. Representative data from at least 3 independent measurements (n = 5–6) are shown. Scale bars, 100 μm.

(B) Pie chart showing the inflammation score of the indicated tissues from the indicated mice at 20 weeks of age. Closed and open circles in Fezf2-TEC-KO and Aire-KO/Fezf2-TEC-KO groups indicate $\beta5t^{iCre/+}$ mice and Foxn1-Cre-transgenic mice, respectively.

(C and D) Inflammation scores (C) and numbers of inflammation foci (D) of the indicated tissues from the indicated mice (n = 7–11) in at least 5 independent measurements at 20 weeks of age. Mean ± SEM is plotted. *p < 0.05, **p < 0.01, ***p < 0.001, ****p < 0.0001. See also Figure S7.

KEY RESOURCES TABLE

REAGENT or RESOURCE	SOURCE	IDENTIFIER
Antibodies		
Anti-mouse CD3ε (clone D4V8L)	Cell Signaling Tech	Cat# 99940; RRID: AB_2755035
APC-eFluo 780 anti-mouse CD4 (clone RM4-5)	eBioscience	Cat# 47-0042-82; RRID: AB_1272183
PE/Cy7 anti-mouse CD4 (clone RM4-5)	BioLegend	Cat# 100528; RRID: AB_312729
eFIuor 450 anti-mouse CD8a (clone 53–6.7)	eBioscience	Cat# 48-0081-82; RRID: AB_1272198
APC-eFluor 780 anti-mouse CD11b (clone M1/70)	eBioscience	Cat# 47-0112-82; RRID: AB_1603193
APC-eFluor 780 anti-mouse CD11c (clone N418)	eBioscience	Cat# 47-0114-82; RRID: AB_1548652
AF594 anti-mouse CD25 (clone PC-61)	BioLegend	Cat# 102045; RRID: AB_2563963
APC-eFluor 780 anti-mouse CD45R/B220 (clone RA-3-6B2)	eBioscience	Cat# 47-0452-82; RRID: AB_1518810
BV421 anti-mouse CD45 (clone 30-F11)	BD Horizon	Cat# 563890; RRID: AB_2651151
PE/Cy7 anti-mouse CD73 (clone TY/11.8)	BioLegend	Cat#127224; RRID: AB_2716103
AF700 anti-mouse CD90.2 (clone 30-H12)	BioLegend	Cat# 105320; RRID: AB_493725
PE/Cy7 anti-mouse TCR-β (clone H57-597)	eBioscience	Cat# 25-5961-82; RRID: AB_2573507
APC-eFluor 780 anti-mouse NK1.1 (clone PK136)	eBioscience	Cat# 47-5941-82; RRID: AB_2735070
PE-Cy7 anti-mouse EpCAM (clone G8.8)	BioLegend	Cat# 118216; RRID: AB_1236471
AF647 anti-mouse Ly51 (clone 6C3)	BioLegend	Cat# 108312; RRID: AB_2099613
PE anti-mouse Ly51 (clone 6C3)	BioLegend	Cat# 108308; RRID: AB_313365
Anti-rabbit Exodus-2/CCL21 (polyclonal)	Bio Rad Laboratories	Cat# AAM27; RRID: AB_2072089
Anti-rabbit DCAMKL1/DCLK1 (polyclonal)	Abcam	Cat# ab31704; RRID: AB_873537
AF488 anti-mouse Aire (clone 5H12)	eBioscience	Cat# 53-9534-82; RRID: AB_10854132
Anti-mouse FEZF2/FEZ1 antibody (clone F441)	IBL	Cat# 18997; RRID: AB_2103205
eFluor 660 anti-mouse Foxp3 (clone FJK-16S)	eBioscience	Cat# 50-5773-82; RRID: AB_11218868
beta tubulin monoclonal antibody (clone BT7R)	Invitrogen	Cat# MA5-16308; RRID: AB_2537819
AF555 anti-rabbit IgG	Invitrogen	Cat# A27039; RRID: AB_2536100
AF488 anti-rabbit IgG	Invitrogen	Cat# A11008; RRID: AB_143165
Anti-Rabbit IgG, HRP	Thermo Fischer	Cat#31460; RRID: AB_228341
Chemicals, peptides, and recombinant proteins		
Pilocarpine hydrochloride	Sigma Aldrich	Cat# P6503
DyLight 594 labeled Ulex Europaeus Agglutinin I (UEA I)	Vector Laboratories	Cat# 1067
Liberase TM	Roche	Cat# 05401127001
DNase I recombinant	Roche	Cat# 04716728001
Percoll	Sigma Aldrich	Cat# 17089101
Ghost Dye Violet 510	Tonbo Biosciences	Cat# 13-0870-T500
2′-Deoxyguanosine hydrate	Sigma Aldrich	Cat# 854999
Formalin solution, neutral buffered, 10%	Sigma Aldrich	Cat# HT501128
Paraformaldehyde solution 4% in PBS	Santa Cruz	Cat# sc-281692
RIPA lysis buffer	Thermo Fischer	Cat# 89900
SDS Protein Gel Loading Solution 2X	Quality Biological	Cat# 351-082-661
Protease/Phosphatase Inhibitor Cocktail	Cell Signaling Tech	Cat#5872
Pierce™ ECL Western Blotting Substrate	Thermo Fisher	Cat#32209

REAGENT or RESOURCE	SOURCE	IDENTIFIER
Critical commercial assays		
Mouse AST ELISA Kit (Aspartate Aminotransferase)	abcam	Cat# ab263882
eBioscience Foxp3/Transcription Factor Staining Buffer Set	Invitrogen	Cat# 00-5523-00
EasySep PE Positive Selection Kit II	STEMCELL	Cat# 17684
EasySep APC Positive Selection Kit II	STEMCELL	Cat# 17681
CD45 MicroBeads, mouse	Miltenyi Biotec	Cat# 130-052-301
PrimeScript™ RT Master Mix	TaKaRa	Cat# RR036
SYBR Premix Ex Taq	TaKaRa	Cat# RR420
Pierce BCA protein assay kit	Thermo Scientific	Cat# 23225
Deposited data		
GSE244501	NCBI Gene Expression Omnibus	https://www.ncbi.nlm.nih.gov/geo
Experimental models: Organisms/strains		
C57BL/6 (B6) mice	The Jackson Laboratory	Strain #:000664 IMSR_JAX:000664
B6-Aire-KO mice (Georg Hollander strain)	Dr. Georg Hollander	Lei et al.[18]
B6-Aire-KO mice (Christophe Benoist strain)	The Jackson Laboratory	Strain #:004743 IMSR_JAX:004743
B6-Ccl21a-tdTomato-knock-in mice	Our facility	Kozai et al.[13]
B6-Relb-KO mice	The Jackson Laboratory	Strain #:002835 IMSR_JAX:002835
B6-Fezf2-flox mice	Dr. Nenad Sestan	Han et al.[46]
B6-Foxn1-Cre-transgenic mice	Dr. Georg Hollander	Zuklys et al.[47]
B6-β5t-iCre-knock-in mice	Our facility	Ohigashi et al.[48]
B6-nu/nu athymic mice	The Jackson Laboratory	Strain #:000819 IMSR_JAX:000819
B6-Pou2f3-KO mice	Dr. Keiko Abe	Matsumoto et al.[72]
Oligonucleotides		
Mouse Gapdh forward primer: 5′-TTGTCAGCAATGCATCCTGCAC-3′	Thermo Fisher	N/A
Mouse Gapdh reverse primer: 5′-GAAGGCCATGCCAGTGAGCTTC-3′	Thermo Fisher	N/A
Mouse Fezf2 forward primer: 5′-ACCCAGCTTCCTATCCCCAT-3′	Thermo Fisher	N/A
Mouse Fezf2 reverse primer: 5′-TCCCTTTTTGGTGAAAGCCT-3′	Thermo Fisher	N/A
Software and algorithms		
FlowJo FACS Analysis software	BD Bioscience	https://www.flowjo.com
BD FACSAria SORP	BD Bioscience	https://www.bd.com
BD LSR Fortessa	BD Bioscience	https://www.bd.com
Zeiss ZEN	Zeiss	https://www.zeiss.com
NIS-Elements	Nikon	https://www.microscope.healthcare.nikon.com
ImageJ	NIH	https://imagej.net
SpectraMax iD3 plate reader	Molecular Devices	https://www.moleculardevices.com

REAGENT or RESOURCE	SOURCE	IDENTIFIER
QuantStudio 6 Flex Real-time PCR System	Applied Biosystems	https://www.thermofisher.com/jp/ja/home/brands/applied-biosystems.html
GraphPad Prism 8	GraphPad Software	https://www.graphpad.com
GraphPad Prism 9	GraphPad Software	https://www.graphpad.com
10x Genomics 3′ Gene Expression v3.1 Dual-Index	10X GENOMICS	https://www.10xgenomics.com
Seurat V3	Hafemeister et al.[73]	N/A
Seurat V4	Stuart et al.[74]	N/A
SingleR	Aran et al.[75]	N/A
Other		
I-A(b) mouse MOG 38–49 GWYRSPFSRWH PE-labeled Tetramer	NIH Tetramer Core Facility	Watanabe et al.[32]
I-A(b) mouse MOG 38–49 GWYRSPFSRWH APC-labeled Tetramer	NIH Tetramer Core Facility	Watanabe et al.[32]
I-A(b) mouse ApoB 978-993TGAYSNASSTESASY PE-labeled Tetramer	NIH Tetramer Core Facility	Nettersheim et al.[33]
I-A(b) mouse ApoB 978-993TGAYSNASSTESASY APC-labeled Tetramer	NIH Tetramer Core Facility	Nettersheim et al.[33]
Polycarbonate Membrane Filter, 0.8 mm Pore Size	Millipore	Cat# ATTP01300
Zone-Quick phenol red thread	Ayumi Pharmaceutical	https://www.ayumi-pharma.com
Novex™ Tris-Glycine Mini Protein Gels, 4–20%, 1.0 mm, WedgeWell™ format	Invitrogen	XP04205BOX